Scientific Research Publishing

Open Journal of Geology, 2024, 14, 403-430
https://www.scirp.org/journal/ojg
ISSN Online: 2161-7589
ISSN Print: 2161-7570

Evaluation of Hydrocarbon Potential Using AVO Analysis in the FORMAT Field, Niger Delta Basin, Nigeria

Charles Chibueze Ugbor, Onyebuchi Samuel Onyeabor, Ifeanyi Celestine Ugwuoke*

Department of Geology, University of Nigeria, Nsukka, Enugu State, Nigeria
Email: *osygodswill@gmail.com

How to cite this paper: Ugbor, C.C., Onyeabor, O.S. and Ugwuoke, I.C. (2024) Evaluation of Hydrocarbon Potential Using AVO Analysis in the FORMAT Field, Niger Delta Basin, Nigeria. *Open Journal of Geology*, **14**, 403-430.
https://doi.org/10.4236/ojg.2024.143019

Received: December 20, 2023
Accepted: March 26, 2024
Published: March 29, 2024

Copyright © 2024 by author(s) and Scientific Research Publishing Inc.
This work is licensed under the Creative Commons Attribution International License (CC BY 4.0).
http://creativecommons.org/licenses/by/4.0/

Open Access

Abstract

The study involved the evaluation of the hydrocarbon potential of FORMAT Field, coastal swamp depobelt Niger delta, Nigeria to obtain a more efficient reservoir characterization and fluid properties identification. Despite advances in seismic data interpretation using traditional 3D seismic data interpretation, obtaining adequate reservoir characteristics at the finest level had proved very challenging with often disappointing results. A method that integrates the amplitude variation with offfset (AVO) analysis is hereby proposed to better illuminate the reservoir. The Hampson Russell 10.3 was used to integrate and study the available seismic and well data. The reservoir of interest was delineated using the available suite of petrophysical data. This was marked by low gamma ray, high resistivity, and low acoustic impedance between a true subsea vertical depth (TVDss) range of 10,350 - 10,450 ft. The AVO fluid substitution yielded a decrease in the density values of pure gas (2.3 - 1.6 g/cc), pure oil (2.3 - 1.8 g/cc) while the Poisson pure brine increased (2.3 to 2.8 g/cc). Result from FORMAT 26 plots yielded a negative intercept and negative gradient at the top and a positive intercept and positive gradient at the Base which conforms to Class III AVO anomaly. FORMAT 30 plots yielded a negative intercept and positive gradient at the top and a positive intercept and negative gradient at the Base which conforms to class IV AVO anomaly. AVO attribute volume slices decreased in the Poisson ratio (0.96 to - 1.0) indicating that the reservoir contains hydrocarbon. The s-wave reflectivity and the product of the intercept and gradient further clarified that there was a Class 3 gas sand in the reservoir and the possibility of a Class 4 gas sand anomaly in that same reservoir.

Keywords

AVO Analysis, Hydrocarbon Potential, Fluid Properties, Reservoir

Characterization, Petrophysical Data, Hampson Russel

1. Introduction

The study of the hydrocarbon reservoir has been an evolving practice in attempt to better characterize it and hence quantify the hydrocarbon resource in a hydrocarbon field. Various attempts had been undertaken by various authors in doing this. [1] [2] investigated the hydrocarborn potential of a reservoir from the vantage of seismic and petrophysical data, even though this provided a good information about the reservoir, the information on the fine fluid constituent was not fully addressed. Also, [3] had performed prospect identification and reservoir characterization using seismic and petrophysical data in "Famito" Field, onshore Niger Delta, Nigeria. This work did not predict the fluid properties within the reservoir. Similarly, [4] performed an assessment of the spectral decomposition techniques in the evaluation of hydrocarbon potential of "BOMS" field, coastal swamp Niger Delta. Also, [5] had studied the characteristics of a hydrocarbon field to establish the hydrocarbon prospectivity and risk analysis using seismic and well log data; These methods could identity a hydrocarbon prospect and quantify the hydrocarbon in place based on available data, but fail to predict the fluid properties of the reservoir from a seismic attribute, like the amplitude variation with offset (AVO) analysis.

Therefore on the other hand AVO is one of the major techniques used on seismic pre-stack data in the oil industry. Seismic amplitudes proved to be rich in rocks and fluid-type information. The availability of hydrocarbon in the subsurface can be linked with anomalous amplitude expressions which make them different from their background, in addition to abnormal frequency responses which result from hydrocarbon attenuation of the seismic waves. These responses of amplitude are characterized using Amplitude Variation with Offset commonly known as AVO.

Seismic and well log integration on 3D seismic data are utilized to analyze the facies and fluid identification which reduces the uncertainty of interpretation in this area. The data integration by the use of AVO technique is suggested as an approach to validate the seismic amplitude anomalies associated with gas sands AVO analysis has been used extensively used in hydrocarbon detection, fluid parameter analysis and lithology characterization [6].

To interpret seismic data, use of quantitative methods is preferred over qualitative methods in the industry. From the various attributes of the shear waves (S) and compressional (P) waves, it is important to be familiar with the behavior of the shear wave and the changes as well as the P-wave, so you can deduce required information and carryout quantitative study in a scenario of different fluids [7]. The characteristic variation of reflected wave pulse which was obtained from a reflector can be analyzed to describe history of a basin, pore fluid, and even rock type in a layer.

Direct hydrocarbon indicator technique using bright spot analysis entails identifying high amplitude anomalous areas in the seismic section in comparison with others [8]. This is the first practical evidence which helped to identify existence of fluid is the "Bright spots" which was noted especially for gas identification in the early 1970. But with future drilling activities showed that there are other geologic cases that exhibit this same amplitude response type according to [9] other than hydrocarbons which will most likely result to a wrong bright spot and lead to a dry hole if drilled. Model-based inversion method and AVO analysis are utilized to derive the rock properties by distinguishing between seismic amplitude scenario for wet gas sands [10].

[11] stated that cross-plotting the intercept and gradient attributes during AVO anomaly investigation would yield a better result. The importance of using this plotting technique the visibility of trends in the data which cannot be seen in a standard amplitude against offset plot (or angle). [12] categorized the gas sands amplitude response enclosed by shales in seismic sections into three classes for clearer identification. With close observation of other behaviors of gas sands, the classification was further developed having a fourth classification. AVO analysis checkmates the transmission coefficients and reflection changes with incidence angle in the seismic data. The rock properties and corresponding AVO responses can be obtained from the well-log data in AVO synthetic modeling which is derived from the seismic rock properties.

[13] used AVO to develop an infill drilling program to increase production. AVO information lowered the risk of finding hydrocarbons by helping to identify seismic events that had a higher probability of being gas-saturated sands, leading to zones of positive AVO which was drilled successfully to reveal commercial quantities of gas, increasing production by 50%.

[14] reviewed the AVO anomalies for gas sands categorized into three classes: Class I, II, and III using the coefficient of the normal incidence reflection (intercept A) P-wave. Class I sands will have a higher impedance sands compared to its overlying shales; this will have a decreasing value of the reflection coefficient (*i.e.* become less positive, implying a decrease) with offset and a positive AVO intercept, while having negative AVO gradient. Class II sands will have minor contrast in impedance; the AVO intercept will be near zero, but may occur as negative or positive. The values of Reflection coefficient may negatively increase or positively decrease with offset, while having a negative AVO gradient. The amplitude of the reflection may then decrease or increase with the offset. Sands with Class III will have a low impedance compared to the overlying shale; with a negative AVO intercept, and a more negative values of the reflection coefficient (which implies an increase) with an offset, resulting to a negative AVO gradient. [15] Young and Tatham (2007) used AVO analysis to discriminate bona fide gas-saturated "bright spots" from brine-saturated "false bright spots". AVO methods were successful at correctly identifying the pore fluid saturant in an average of 90% of the 20 prospective intervals as opposed to 45% using "bright spot" analysis alone. [16] used AVO analysis for detecting free gas zone in Heuksan

Basin. On the cross plotting of gradient and intercept, AVO anomaly appeared in first and third quadrant which means a typical natural gas layer (Class III).

[17] used AVO analysis modeling in hydrocarbon exploration and were able to successfully obtain the gassy sand anomalies from the AVO attributes. [18] employed the concept of AVO technique in understanding the lithologies and pore fluids in Niger Delta reservoirs. The cross-plot analysis technique was used to detect a low-impedance gas sand reservoir with class III anomaly being associated with the hydrocarbon sands. To demonstrate how useful the AVO cross-plotting technique is in AVO analysis. [19] defined Class IV sands using a combination of gradient and intercept for the scenario where a reflection coefficients initially negative become less negative with an increasing offset, resulting to a negative intercept and a positive gradient.

Therefore, to determine the precision of the anomaly as a result of changes in lithology and fluid content, the technique of utilizing AVO analysis is doing a comparison between the synthetic seismic models (standard condition) with existing real data. [20] used well logs and 3D seismic to evaluate the hydrocarbon trapping potential and 3D structural analysis of subsurface structures of Otu Field, Niger Delta with the aid of the log data, network of faults, horizon delineation, and extraction of the RMS amplitude which shows that field contains hydrocarbon economically. [21] predicted the reservoir system quality at Kwe field Niger delta and identified its depositional environment using the petrophysical properties of the reservoir and well-log data. He identified 7 reservoirs in the Kwe field.

[22] with an objective to identify new prospects did an evaluation of the Olive field in Niger Delta using well logs, check shots and 3D seismic data. He established the time and depth structural maps, porosity ranging from 24.63% - 34.01%, hydrocarbon saturation ranging from 70.93% - 78.86% with seismic interpretation showing the field to be well faulted and seismic amplitude attribute maps characterized by high amplitude range (bright spot) in the zone surrounded by the structural traps and hence the identification of Four hydrocarbon prospects in the field.

[23] used AVO analysis for carbonate and naturally fractured reservoirs exploration and characterization to demonstrate that AVO technique is applicable in different geological settings and environments including old and deep sand reservoirs in North Africa and the Middle East. [24] used well-log analysis and some petrophysical properties like water saturation, porosity, permeability, bulk water, Net to gross, and hydrocarbon saturation to estimate the hydrocarbon prospect of the site and identified 4 sand reservoirs.

The major aim of AVO analysis in the Niger Delta is to derive subsurface rock properties in the area using a combination of well log data and the conventional surface seismic data. The derived rock properties will aid in the determination of lithology, porosity and fluid saturation. Previous works carried out using AVO have shown that geological formations containing hydrocarbons have its own amplitude in which they respond to seismic excitations; these seismic responses

are mainly guided by its pore spaces, fluid content and lithology type. This can also help in interpreting the strong amplitude anomalies which are seen at top of saturated hydrocarbon reservoirs and yielded successful AVO analysis in many basins around the world [25]. However, a good number of drilled wells have reportedly failed both in the Niger Delta Basin and other basins due to a poor understanding of the reservoir properties in advance of drilling. Conducting an AVO analysis has proven useful in better illuminating the reservoir through a more efficient characterization of the reservoir and identifying the fluid properties. Therefore AVO analysis along with its attribute analysis will assist in solving such a problem.

Some exploration using 3D seismic data in Niger Delta Basin had focused on bright spots or anomalously large negative amplitudes in rocks. However this had sometimes yielded surprising disappointing results especially in areas impregnated by highly cemented sands often calcite cement in thin pinch-out zones, low-porosity heterolithic sands and over-pressured zones. In his study of the hydrocarbon reservoir, [2] had used both seismic and well data to successfully evaluate the hydrocarbon reservoir in the SIMA field of the Niger Delta. Similarly, [4] had also attempted successfully to evaluate the hydrocarbon potential of BOMS field in the Niger Delta using spectral decomposition method. It thus becomes necessary to deploy, in this study, the use of AVO analysis to evaluate the reservoir to assess the performance in the characterization and identification of the fluid properties by integrating the AVO attributes.

An approach in this study is to identify the AVO classes present in the reservoir using intercept and gradient analysis alongside AVO attributes such as scaled poisson ratio and s-wave reflectivity using a case study of FORMAT field Niger Delta. Essentially, the approach will solve a set of objectives such as to delineate the reservoir in the study area by integrating the seismic and AVO synthetic modeling, perform an intercept and gradient analysis, apply a real data analysis on the seismic data and identify the reservoir fluid properties using the AVO and its attributes. Consequently, the result is intended to better illuminate the reservoir characteristics including fluid properties than traditional seismic data interpretation process that had sometimes resulted in disappointing results. Integrating the AVO analysis would thus improve confidence in decision-making for citing production wells and avoiding dry hole due to inadequate or imprecise reservoir characterization.

1.1. Geology of the Study Area

The Niger Delta Basin is known as an extensional rift basin which is found in Gulf of Guinea and projects throughout Niger Delta Province. **Figure 1** shows the geologic map of the Niger Delta. The basin lies on the passive continental margin which is near the western coast of Nigeria. The delta has southwestward progradation from Eocene to the Present, which formed many of the depo-belts representing the main active part of the delta at every development stage [26].

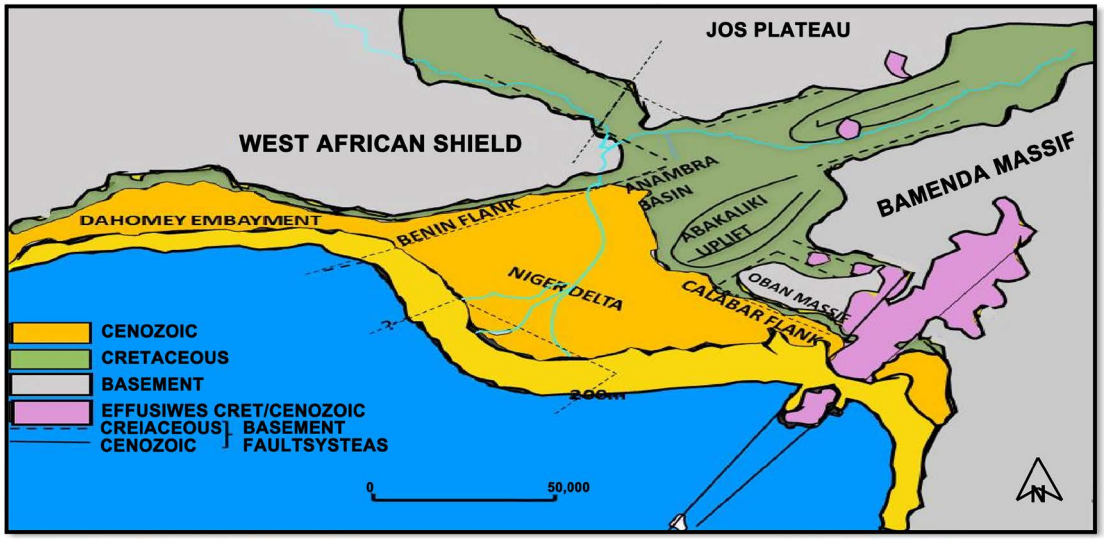

Figure 1. Geologic map of the Niger Delta (redrawn from [33]).

The sediment's mean thickness is approximately 10 km at the center of the depo-belts and the volume of the sediment is estimate as 500,000 km^3 [27]. Province of Niger Delta has one identified petroleum system. [28] [29] noted this as the Akata-Agbada Petroleum System (Tertiary Niger Delta). [30] further researched and also concurred to one petroleum system within the Niger delta, formed during the southern Atlantic opening at the triple junction which started during the late Jurassic and continued to Cretaceous. Based on [28], the delta began to develop in the Eocene with sediment accumulation which now has a thickness of about 10 km. The area is made up of a sedimentary basin geologically which basically has three Formations: Benin Formations, Agbada, and Akata. The Akata Formation comprises shale which is formed during the marine transgressive cycle and is the major source rock in this basin [30]. Agbada Formation is predominantly made of sand deposited in a paralic environment.

This makes up the oil and gas reservoir that is within the basin [31]. Agbada Formation is referred to by [32] as a zone of transition with intercalation of shale and sand. The Agbada Formation has hydrocarbon traps which mostly occur as rollover anticlines in growth faults (dip closures) and some stratigraphic traps.

The faults are mostly listric and also form major barriers leading to accumulated hydrocarbon compartmentalization. Benin Formation stratigraphically covers the upper part of the Delta and lies above Agbada Formation. It consists of unconsolidated sands approximately 2000 m thick [34]. It is made up of coastal plain sands as it is deposited in a fluvial environment. **Figure 2** is a map showing the location of the study area, FORMAT field and the study wells locations.

1.2. AVO Principles and Classification

AVO is the comparison of seismic amplitude changes compared to the offset of the traces from the source (that is the shot point). Hence, is called Amplitude

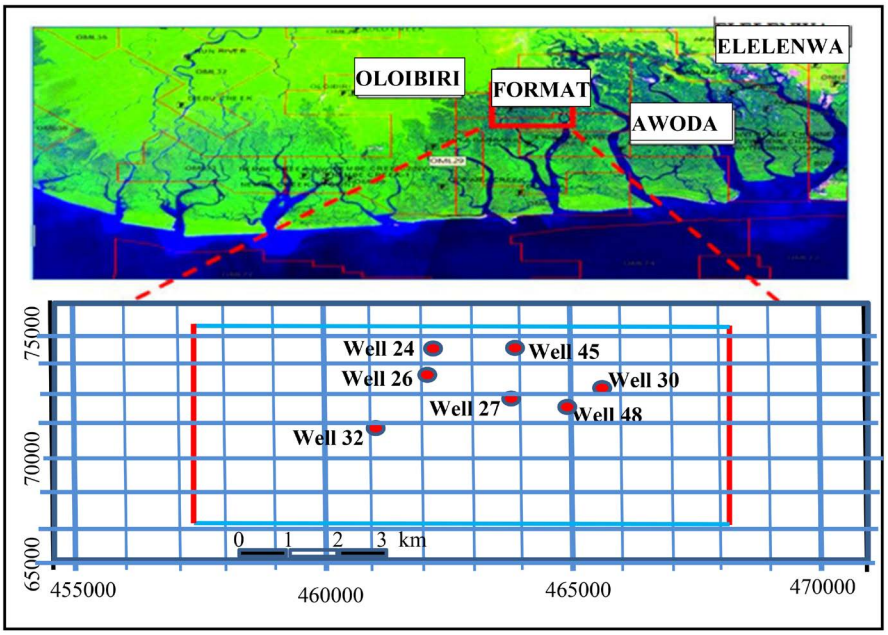

Figure 2. Map of FORMAT field location in Niger Delta and base map of the study area with seven wells.

variation with Offset (AVO). It was first proposed by [35]. It is commonly used to estimate the P-wave and S-wave velocities. AVO allows us to determine S-wave response without actually using an S-wave recorder, by accounting for the differences between the P-wave and S-wave over the offset.

The Aki-Richards approximation is widely accepted and used to compute AVO attributes, namely, the zero-offset reflections called intercept and the rate of change of the amplitude from angle to another called gradient. With these two attributes the amplitude can be formulated at different angles as expressed by [7] equation as shown in Equation (1)

$$R(\theta) = R_p + G\sin^2\theta \tag{1}$$

$R(\theta)$ is the reflection coefficient at angle at theta, R_p = the intercept at zero-offset (that is, true P-wave reflectivity), while G = gradient of the amplitude-offset plot. This equation is applicable up to 30 degrees.

AVO technique is the analysis of the variations of the amplitude as a function of offset. The amplitude varies with offset because the reflection coefficient varies when the angle of incidence of the wave at the interface varies. These variations are governed by the contrast in P-wave velocity and S-wave velocity at the interface. When there is gas in the layer, Vp drops whereas Vs does not change or increases due to influence of gas as in figure. This means that Vp/Vs is anomalous, and we hope to see the effect of this anomaly in the reflection pattern. By modeling the AVO effects for different reservoir fluids, AVO responses in seismic data can be predicted. The AVO response is dependent on three parameters; the P-wave velocity, the S-wave velocity and the density in a porous reservoir rock.

In this study, the synthetic approach in AVO techniques will is employed to distinctively understand the fluids effects on the seismic reflections. This approach is discussed in details as a part of AVO analysis especially to interpret the real data.

The VS is estimated from VP using the empirical relationship between the two, the [36]'s relation given as in Equation (2);

$$\text{S-wave} = C_1 \times \text{P-wave} + C_2 \tag{2}$$

where C_1 = constant = 0.86190, C_2 = −1172.0000.

In AVO synthetic modeling, the P-wave, S-wave and density logs used to generate the synthetics for different fluid scenarios in the selected reservoir sand. These scenarios for pure gas, pure oil and pure brine are based on 100% substitution for each case. However, using the two-term version of Equation (2), R_p and G, representing the intercept and gradient of the AVO curve respectively according to [7]; synthetics are then generated for the different fluid cases, where the top sand amplitude increases negatively for gas and oil as it positively increased for brine with increase in offset at the base. The AVO response curves are plotted and interpreted for the top of the reservoir sand unit at the boundary between the shale and porous sand as applied in this study in succeeding chapter.

[9] identified three well-defined classes of gas sand responses by plotting amplitude against normal-incidence reflection coefficient angles and they came out with class I, II and III (However, [36] used the principles of AVO cross plotting to add a class IV gas sand by suggesting that shale overlying sandstone bearing hydrocarbon should be classified according to their location on the A and B plot plane, instead of by the normal incidence reflection coefficient alone. **Figure 3** shows the classification chart of the AVO.

Reflection coefficient of P-wave at normal incidence is strongly positive and shows a sharp decrease in amplitude with offsets, and a possible a phase change at far offsets. There are also hydrocarbon-rich sands, which prevents water to

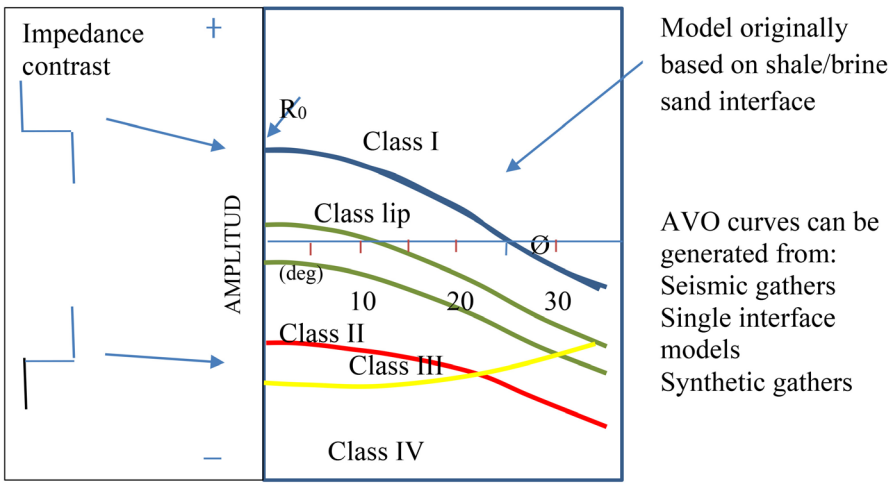

Figure 3. Classes of AVO after [9] [11] and [37].

penetrate the surface. They are more common in deep reservoirs than shallow ones (Figure 3).

AVO Class II

Where there is a strong phase difference at near or moderate offsets, and the normal incidence coefficient is slightly positive (class IIp), when the small amplitude of the primary reflected has a large variation in AVO response. This corresponds to a near-zero impedance contrast (Figure 3).

AVO Class III

Is an excellent example of a bright spot. In this case, the shale is on top of the gas sands that has a lower negative reflection coefficient. In shallower formations or reservoirs that haven't been glued together, these bright spots can be found (Figure 3). This corresponds to lower impedance gas sands.

AVO Class IV

This is a rare type of AVO response with soft reservoir gas sands overlain by relatively hard cap-rock shales. It has negative reflection coefficient at zero offset and lower impedance with amplitude which decreases against the offset (Figure 3). An AVO classification model by the gradient and intercept crossplot is shown in Figure 4.

2. Materials and Method of Study

2.1. Materials

The data utilize in this work are well logs data gotten from FORMAT field in the coastal-swamp depobelt within Niger Delta basin obtained from SPDC Port Harcourt. These data were analyzed with Hampson Russell Software (HRS). This includes the 3D pre-stack time migrated seismic volumes and suite of well log profiles (gamma ray, caliper, Resistivity, density, and P-wave).

The wells are vertically drilled and two (FORMAT 26 and 30) has full suites of

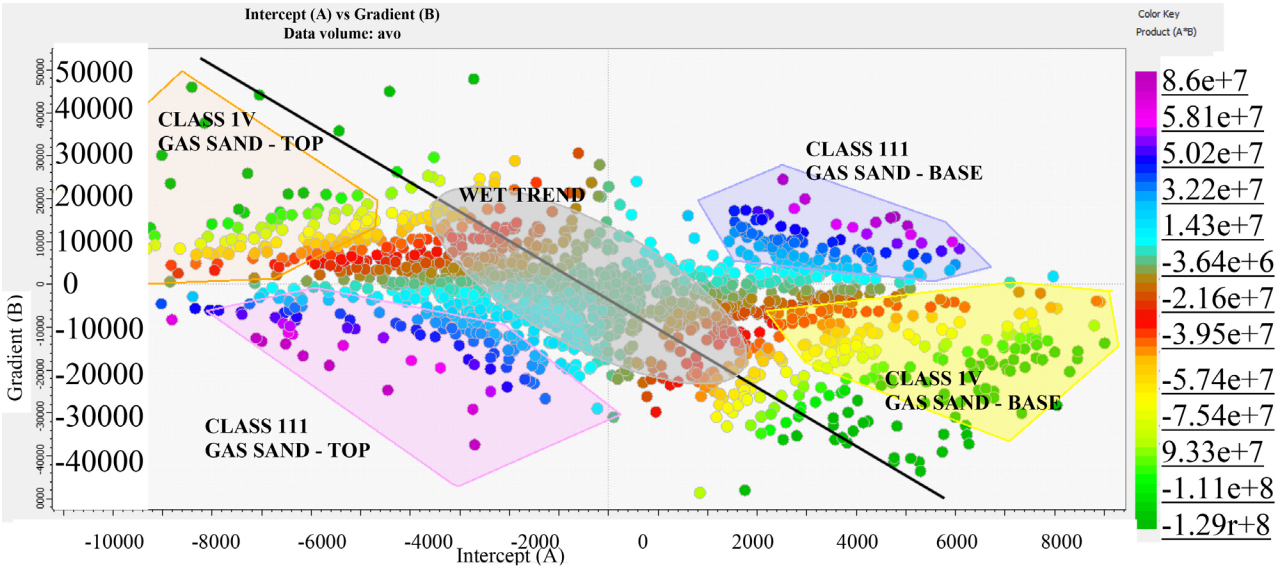

Figure 4. Gradient and intercept cross plot the AVO classification model.

wireline logs over the intervals of the reservoir. FORMAT 25 is located in the Southwest of the field has a total depth of 11,661 ft and FORMAT 30 situated Southeast of the field totals 12,000 ft with full suites of wireline logs. Out of these two wells, the gamma-ray is consistent with the shale sand sequence of the Niger Delta as the resistivity log reflects its characteristics at the regions of sand and shale sequences. Table 1 shows the available well logs in the wells used for the study, FORMAT 26 and FORMAT 30. Figure 5 and Figure 6 show the available well logs at the well locations at FORMAT 26 and FORMAT 30 respectively.

2.2. Method of Study

The study was carried out by running a set of analyses using the well and seismic data and following a set of procedure as follows:

2.2.1. Selection of Reservoir Interval and Wells

Well-log suites are basically analyzed to describe zones of interest depending on

Table 1. Suite of well logs used for the study.

WELL	Gamma Ray (API)	Caliper (in)	Resistivity (ohm)	Density (g/cc)	P-wave (ft/s)	S-wave (ft/s)	Total Depth (ft)
FORMAT 26	Yes	Yes	Yes	Yes	Yes	No	11,661
FORMAT 30	Yes	Yes	Yes	Yes	Yes	No	12,197

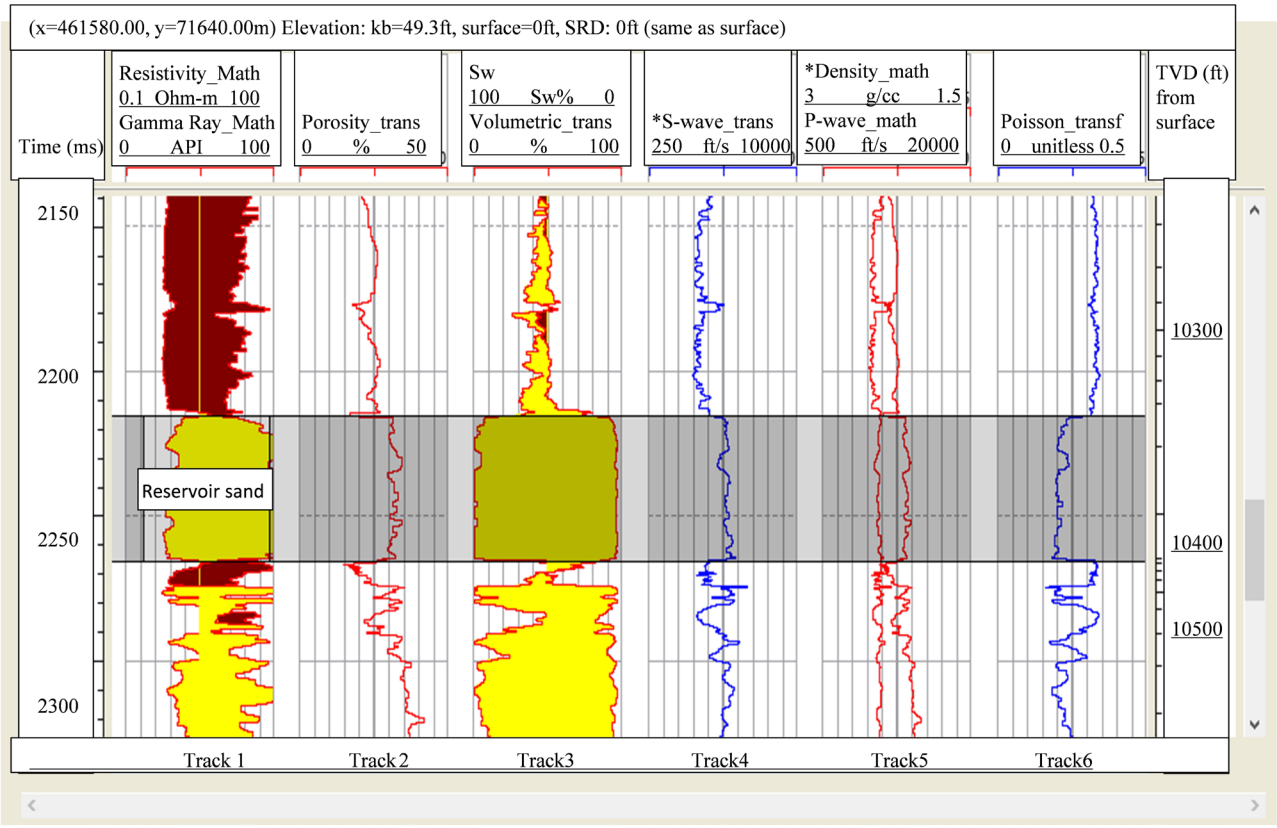

Figure 5. Reservoir parameter crossplots showing the reservoir sand delineation at FORMAT 26.

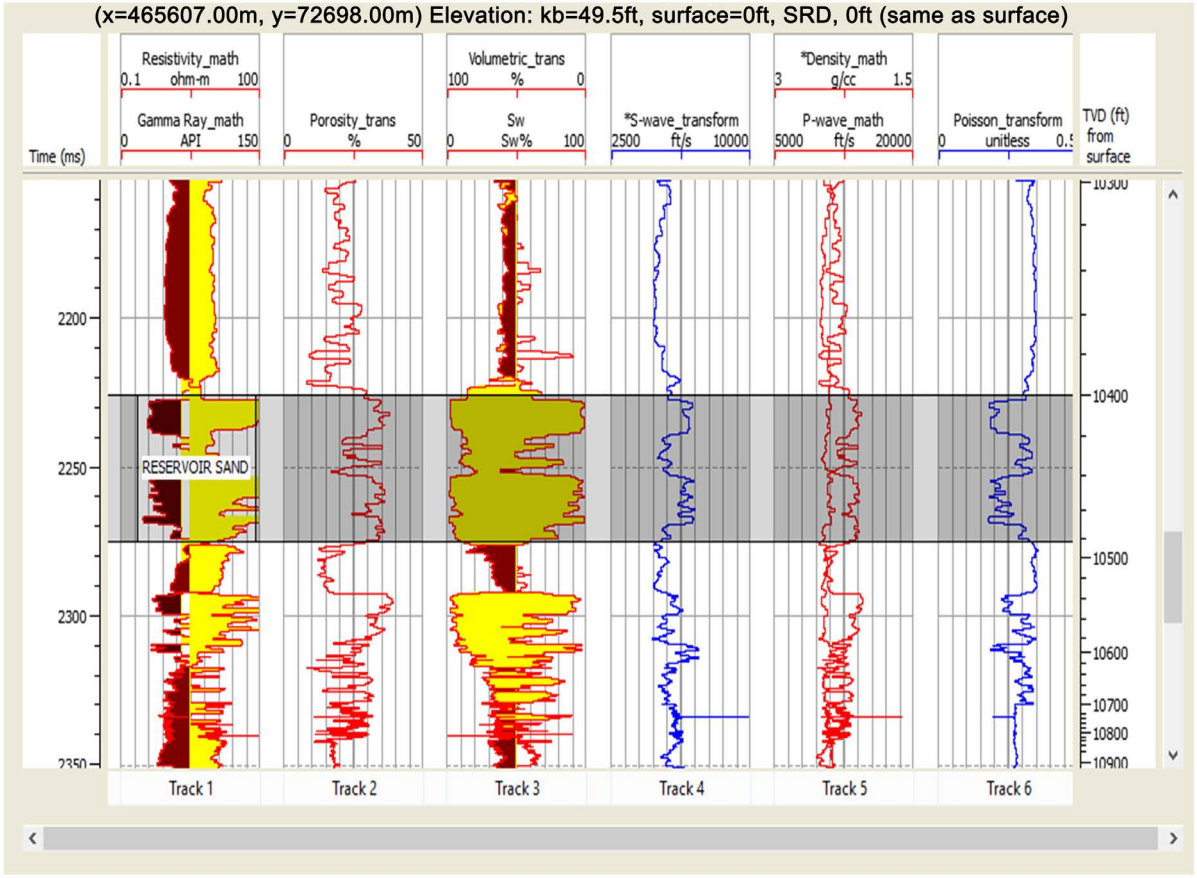

Figure 6. Reservoir parameter crossplots showing the reservoir sand delineation at FORMAT 30.

the behavior of Resistivity logs and gamma rays. In this, the delineation of target zones becomes paramount to estimating the thickness or potentiality of a formation. To get this, a gamma-ray log was colour-coded with two colours: yellow reflecting a decline in gamma-ray equivalent to sand (cutoff < 65 API) and a brown colour reflecting an increase in gamma-ray which indicates shale zone (cutoff > 65). In addition, within the sand reservoir (95 ft and 126 ft in both wells), sand intercalations and a small amount of shale but on top of the reservoir were very evident, shale thickness is larger across the wells which possibly functions as cap rocks. **Figure 5** and **Figure 6** show the log crossplot of reservoir showing the reservoir sand delineation at FORMAT 26 and 30 respectively.

2.2.2. Seismic Data Conditioning

Reservoir characterization needs seismic data conditioning to be free from noise, align time across all the angles, and minimizes amplitude damaging effects [38] [39]. A Seismic data that is poorly processed and only focused on data image quality improvement for stratigraphic and structural interpretation can majorly affect the inversion algorithm results of the rock properties and also the final interpreted result ultimately. From several studies, it was observed that amplitude friendly (reservoir-compliant) processed data has a notable effect on the data behavior which is interpreted in the AVO attributes (gradient and intercept)

domain. For effective and noise-free data to serve as input to spectral decomposition and AVO algorithm, the following data conditioning procedures were applied: amplitude-offset scaling, time-misalignment correction, and conversion from offset stack to angle stack for pre-stack inversion.

For FORMAT seismic, there are near and far offset stacked data with full-stack seismic data. A 3D arbitrary section of the full stack seismic data with arbitrary line cutting across FORMAT 26, and 30 were created. This data served as the input for spectral decomposition.

By calculating the average reflection angle for each of these offsets or simply using the already established approach in Hampson Russel 10.3 version, it was possible to create offset and angle gathers. Thus, the arbitrary seismic data was transformed from post-stack to seismic offset and angle gathers for AVO analysis. In the angle-gather, each seed trace has a corresponding constant incidence/reflection angle.

In AVO analysis, the offset data is first converted to angle gathers where the velocity data used in our research have been derived from the well data. The benefit of angle gathers is to plot the offset against the incidence angles in order to verify the limit of the far offset or far angles that can be trusted.

Figure 7 and Figure 8 show conditioned angel gathers of 3D arbitrary near to far angle stacks with p-wave curve pilot at 1693 inline of FORMAT 26 and FORMAT 30 showing the angle range. In these figures, three angle traces represent the near (green - yellow), mid (red - cyan) and far (blue - purple) angle stacks of 0˚, 20˚, and 30˚ respectively. Equation (1) is applicable up to 30˚.

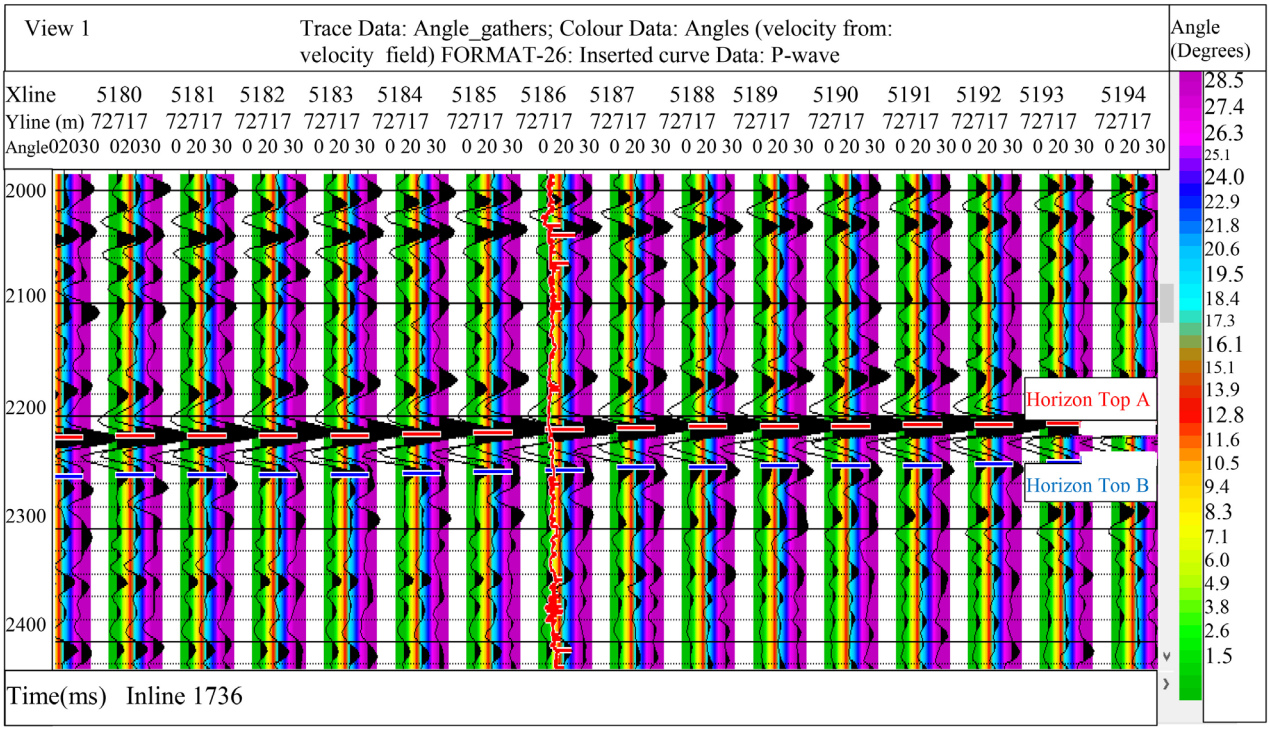

Figure 7. Conditioned angle gathers of 3D arbitrary near to far angle stacks with P-wave curve plot at 1693 Inline of FORMAT 26 showing incident angle range.

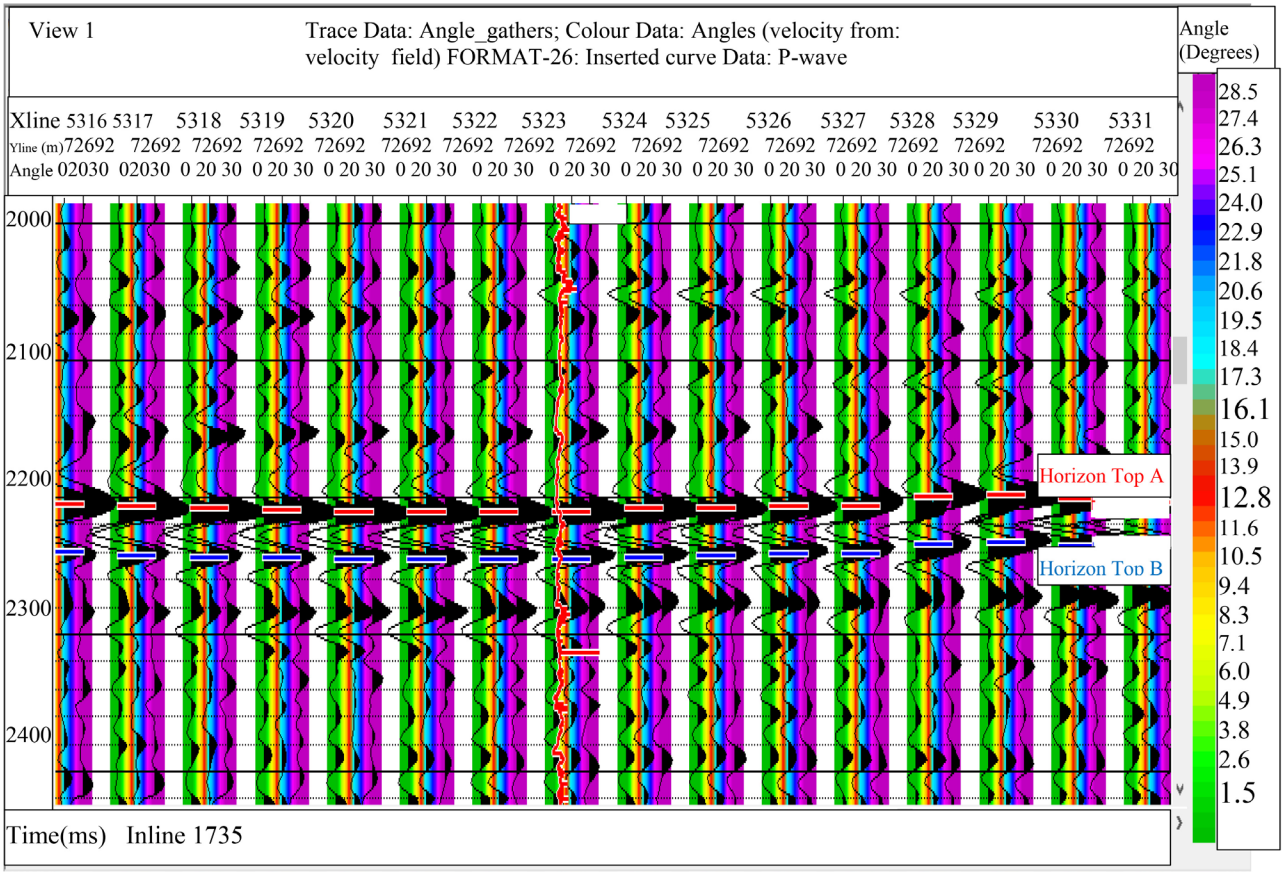

Figure 8. Conditioned angle gathers of 3D arbitrary near to far angle stacks with P-wave curve plot at 1693 Inline of FORMAT 30 showing incident angle range.

3. Results and Discussion

3.1. AVO Synthetic Modeling

The two term equation from [7]'s study was employed to create the synthetic gathers through the substitution of different fluids at 100% for elastic parameters (ρ, VS, and VP). The output of the fluids substitution in form of synthetic are Pure Gas (view 1), Pure Oil (view 2), and Pure Brine (view 3) for FORMAT 26 and 30.

The base and the top of the target zone at different fluids synthetic, around 2232 ms - 2251 ms (pure gas), 2233 ms - 2251 ms (pure oil), and 2232 ms - 2250 ms (pure brine), were plotted as AVO curves and gradient and intercept crossplot space using the two-term Aki and Richard's (1980) equation. The pure gas AVO curves increase (brightening) with an increase in offset (red curve-top) as the base curve dims with an increase in offset (green curve). The gas sand's top plots at the class III position as the base plots opposite it having negative intercept (A = −0.0550) and gradient (B = −0.1137). The pure oil AVO curves increase (brightening) with an increase in offset (blue curve-top) as the base curve dims with an increase in offset (cyan curve). The top of this oil sand plots at the class II position as the base plots opposite it having negative intercept (A = −0.0375)

and gradient (B = −0.1569). The pure brine AVO curves increase (dims) with an increase in offset (yellow curve-top) as the base curve dims with an increase in offset (brown curve). The top of this oil sand plots at the wet trend position as the base plots opposite it having positive intercept (A = 0.1553) and a negative gradient (B = −0.4489). The same analysis is applicable for FORMAT 30. The curve parameters for different scenarios for FORMAT 26 and 30 are shown in Table 2 and Table 3 respectively. Figure 9 and Figure 10 show the synthetics for pure brine, pure oil and pure gas cases showing the fluid substitution model for FORMAT 26 and FORMAT 30 respectively.

Further analyses consist of a crossplot and scatterplot of the intercept versus gradients of the data from both wells, FORMAT 26 are shown in Figure 11 and Figure 12 respectively. The curves show for the pure brine (right), pure oil (middle) and pure gas (left) cases showing the AVO class synthetic models.

Similarly, a crossplot and scatterplot of the intercept versus gradients of the data from wells, FORMAT 30 are shown in Figure 13 and Figure 14 respectively. This applies for both top and bottom, for the pure brine (right), pure oil (middle) and pure gas (left) cases the AVO class synthetic models. Table 2 and Table 3 show A and B curves parameters for different synthetic scenarios for FORMAT 26 and 30 respectively.

Table 2. Shows A and B curves parameters for different synthetic scenarios for FORMAT 26.

FORMAT 26	A (Intercept)	B (Gradient)	Correlation (%)	Time (ms)	Sand Interval
Pure Gas = 100%	−0.0550	−0.1137	0.9865	2232	**Top**
	0.0962	0.0651	0.9938	2251	**Base**
Pure Oil = 100%	−0.0375	−0.1569	0.9810	2233	**Top**
	0.0890	0.1007	0.9929	2251	**Base**
Pure Brine = 100%	0.01553	−0.4409	0.9995	2232	**Top**
	−0.0914	0.3851	0.9895	2250	**Base**

Table 3. Shows A and B curves parameters for different synthetic scenarios for FORMAT 30.

FORMAT 30	A (Intercept)	B (Gradient)	Correlation (%)	Time (ms)	Sand Interval
Pure Gas = 100%	−0.0579	−0.1274	0.9857	2217	**Top**
	0.0580	0.0656	0.9924	2238	**Base**
Pure Oil = 100%	−0.0414	−0.1586	0.9835	2218	**Top**
	0.0550	0.0977	0.9918	2235	**Base**
Pure Brine = 100%	0.0462	−0.3125	0.9979	2219	**Top**
	−0.0128	0.1003	0.9988	2242	**Base**

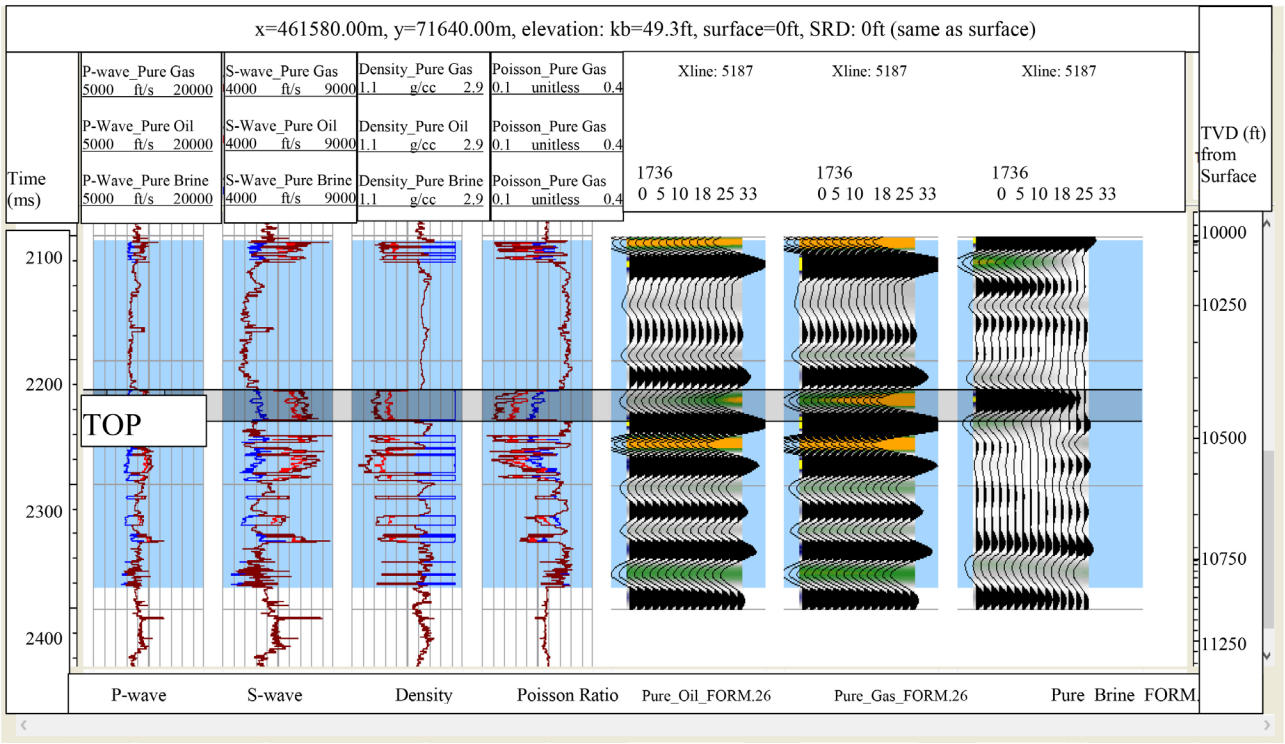

Figure 9. Synthetics for pure brine, pure oil and pure gas cases showing the fluid substitution model for FORMAT 26.

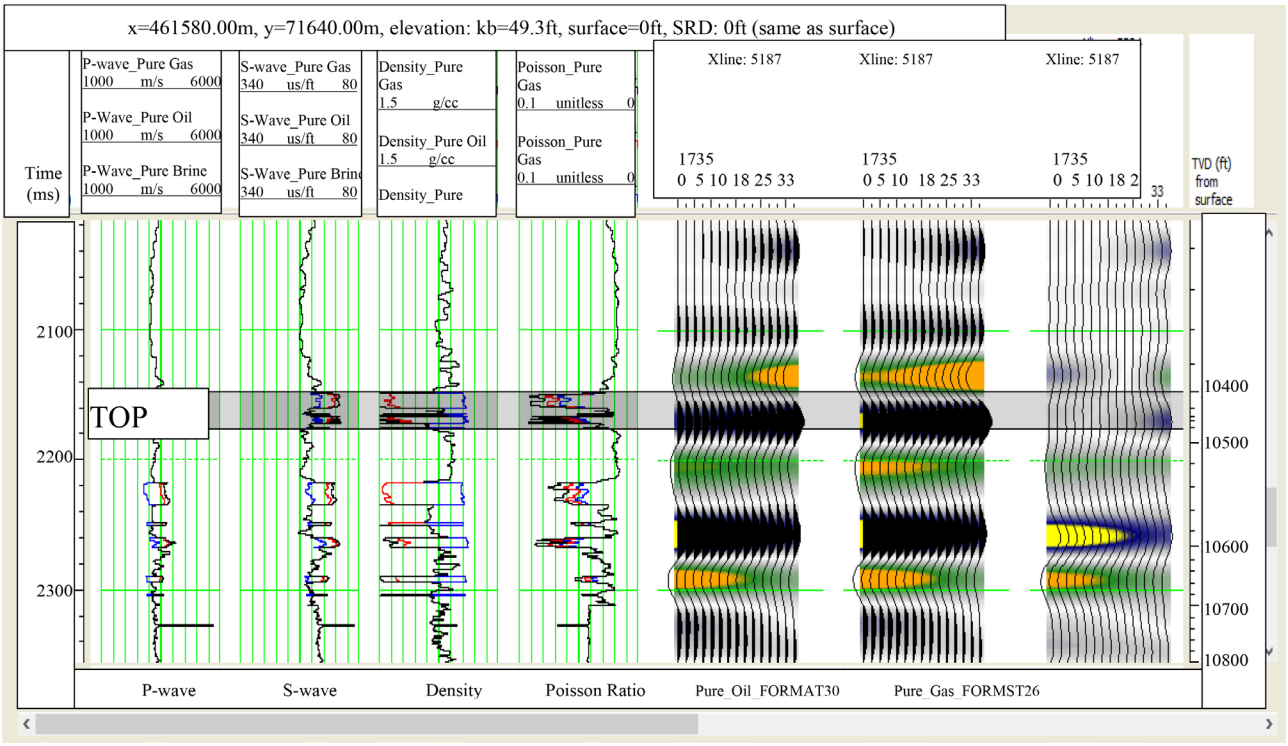

Figure 10. Synthetics for pure brine, pure oil, and pure gas cases showing the fluid substitution model for FORMAT 30.

This model will be used to interpret the real seismic model. To create synthetics, the system convolves P-wave pure gas, S-wave pure gas, and Density pure

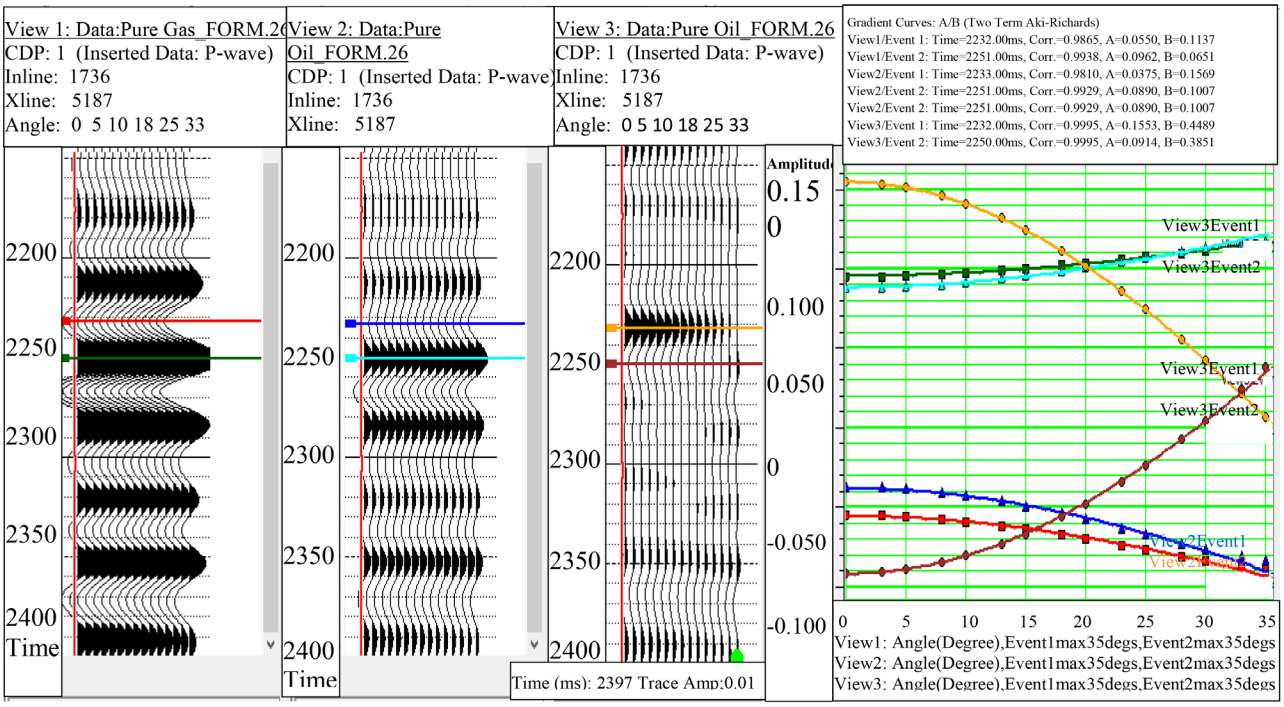

Figure 11. Crossplot of Intercept vs Gradient for FORMAT 26 for both top and bottom) for the pure brine (right), pure oil (middle) and pure gas (left) cases showing the AVO class synthetic models.

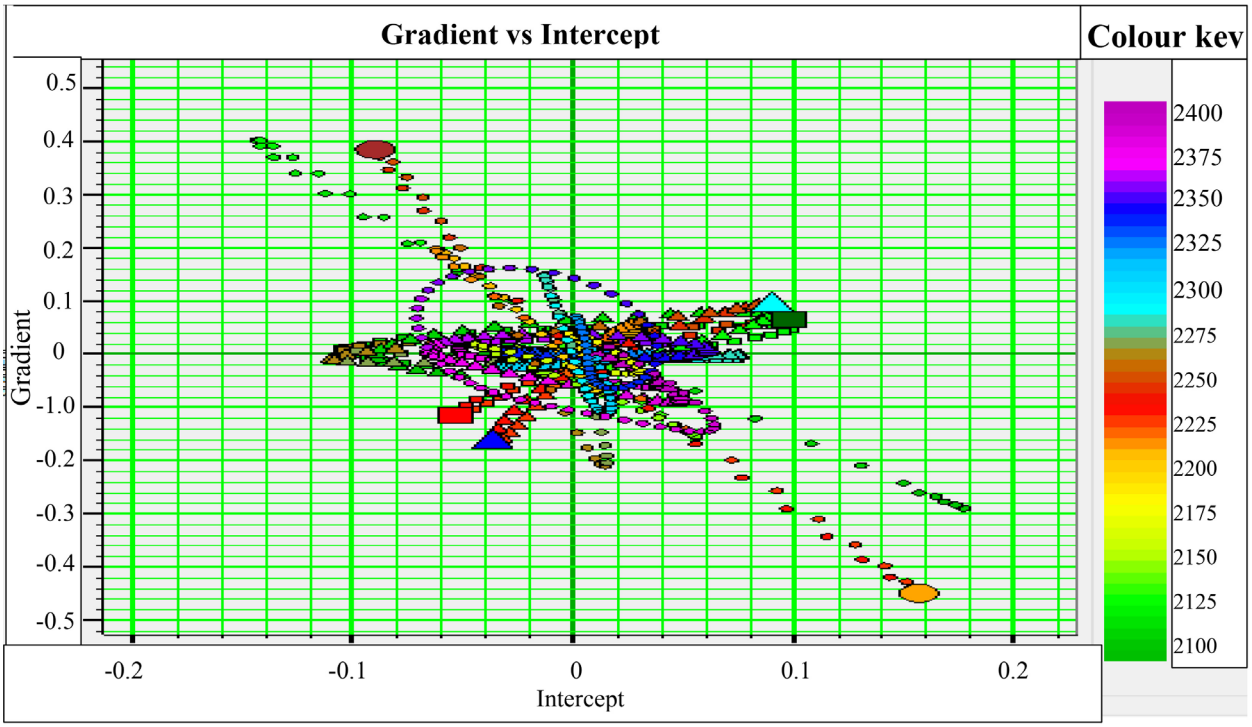

Figure 12. Scattered plot of Intercept vs Gradient (FORMAT 26) for the pure brine (yellow), pure oil (blue) and pure gas (red) cases showing the AVO class synthetic models.

gas. This gives the pure gas of FORMAT 26, same applies to pure oil and pure brine.

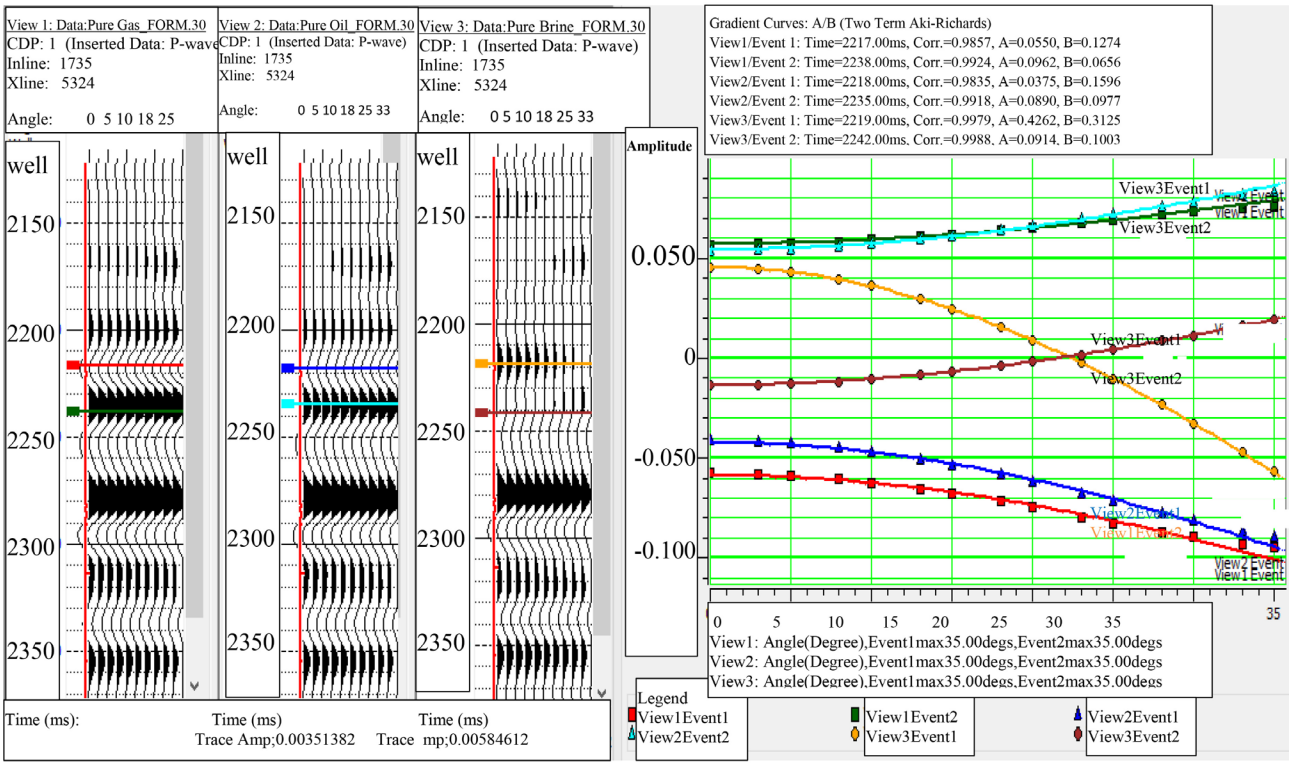

Figure 13. Crossplot of Intercept vs Gradient (FORMAT 30) for both top and bottom) for the pure brine (right), pure oil (middle) and pure gas (left) cases the AVO class synthetic models.

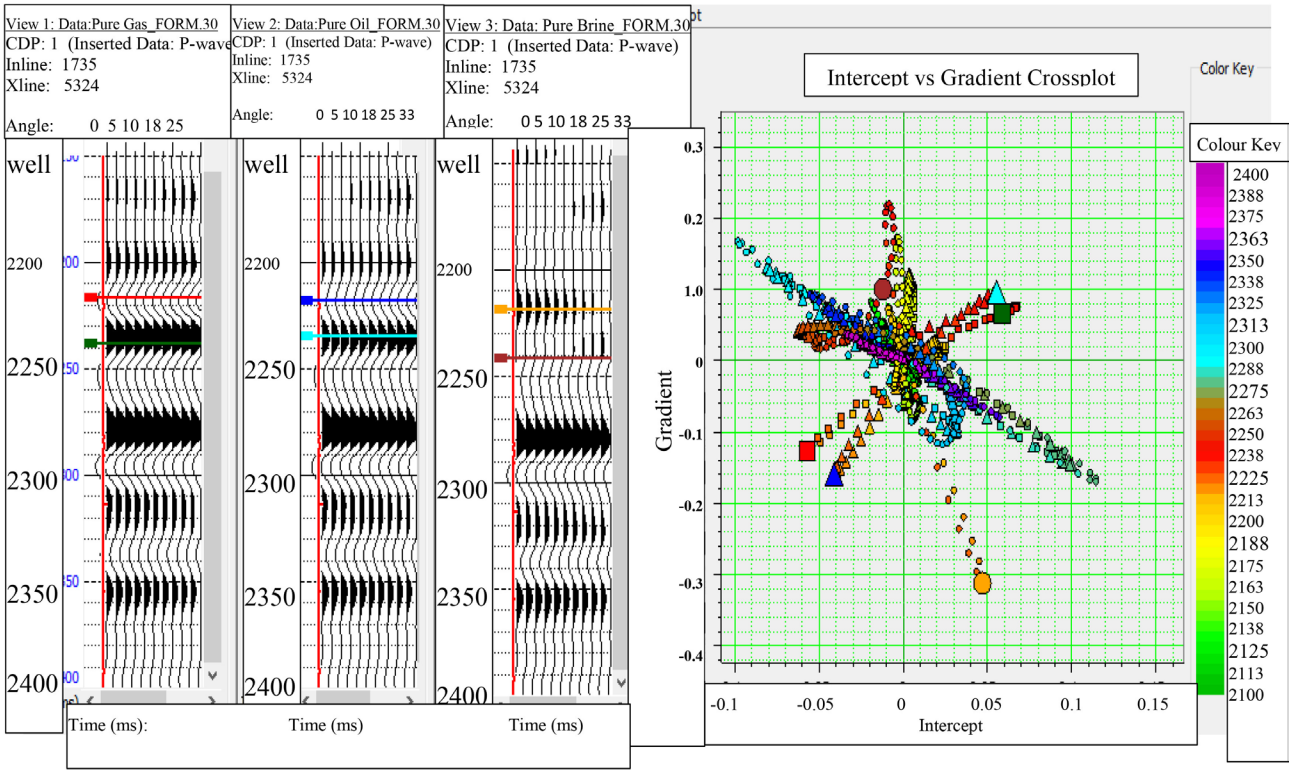

Figure 14. Scattered plot of Intercept vs Gradient (FORMAT 30) for the pure brine (yellow), pure oil (blue), and pure gas (red) cases the AVO class synthetic models.

So, in the reservoir, the top Amplitude decreases and the base Increases both for gas and oil but that of gas is sharper while it is the reverse for brine.

3.2. Application of AVO on Seismic Data

From the seismic gathers, the Near (0), Mid (20) and Far (35) offset gathers were created. From the data it was observed where the Top and Base were plotting. This was the similar effect as seen on the seismic synthetics. The following figures illustrate the results from the AVO analysese on the seismic data.

Figure 15 is an AVO scattered plot showing the Intercept (A) vs. Gradient (B) curves for FORMAT 26 for both top and bottom) of the pure oil top (blue) and pure gas top (red) cases. Figure 16 is an AVO crossplot showing the Intercept (A) vs. Gradient (B) for FORMAT 26 for both top and bottom) of the pure oil top (blue) and pure gas top (red) cases. Similarly, the same AVO analysis was performed on the FORMAT 30. Figure 17 is an AVO scattered plot showing the Intercept vs Gradient (VOM 30 for top and bottom) of the pure oil top (blue) and pure gas top (red) cases while Figure 18 is an AVO cross plot showing the Intercept vs Gradient (VOM 30) for both top and bottom) of the pure oil top (blue) and pure gas top (red) cases. Also, Figure 19 is a crossplot for the intercept vs. gradient, illustrating the categories of different gas classes (III & IV) while Figure 20 is an AVO crossplot superimpose on the volume showing two AVO anomalies of gas sand (class III and IV) of FORMAT sands at the FORMAT 26

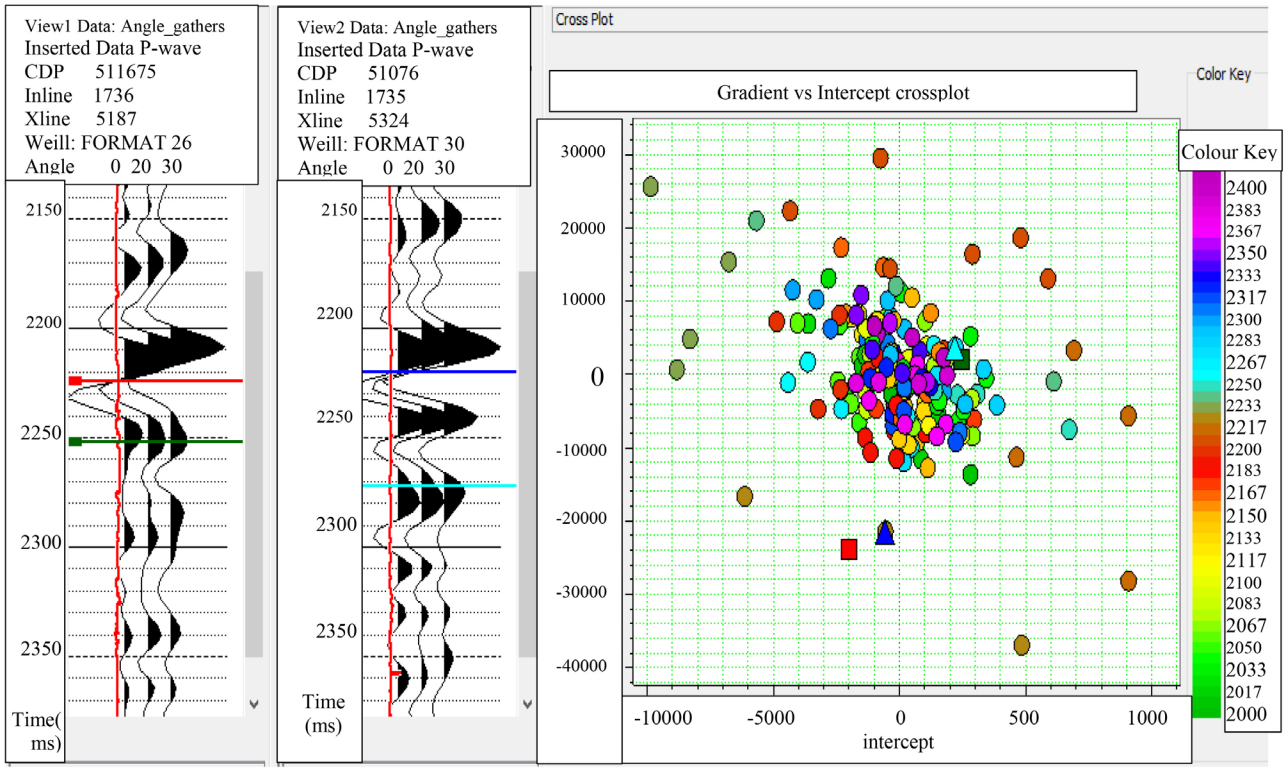

Figure 15. AVO scatter plot showing the Intercept (A) vs. Gradient (B) curves for FORMAT 26 for both top and bottom) of the pure oil top (blue) and pure gas top (red) cases.

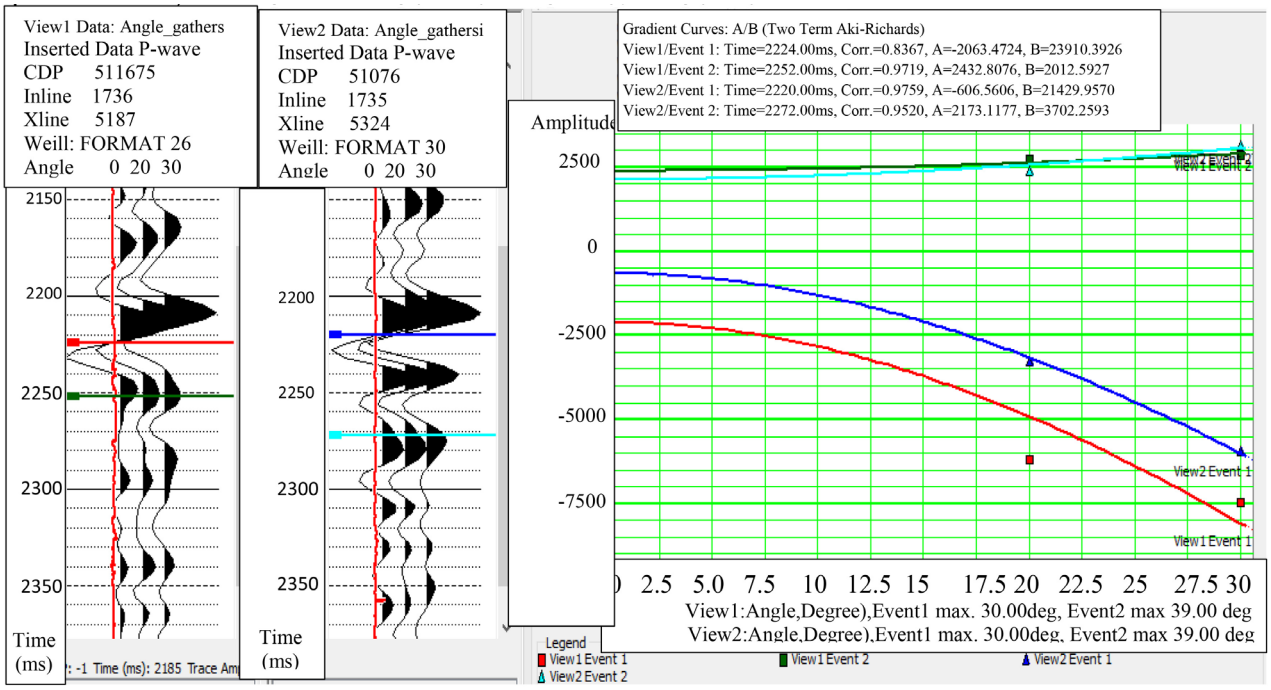

Figure 16. AVO cross plot showing the Intercept (A) vs. Gradient (B) for FORMAT 26 for both top and bottom) of the pure oil top (blue) and pure gas top (red) cases.

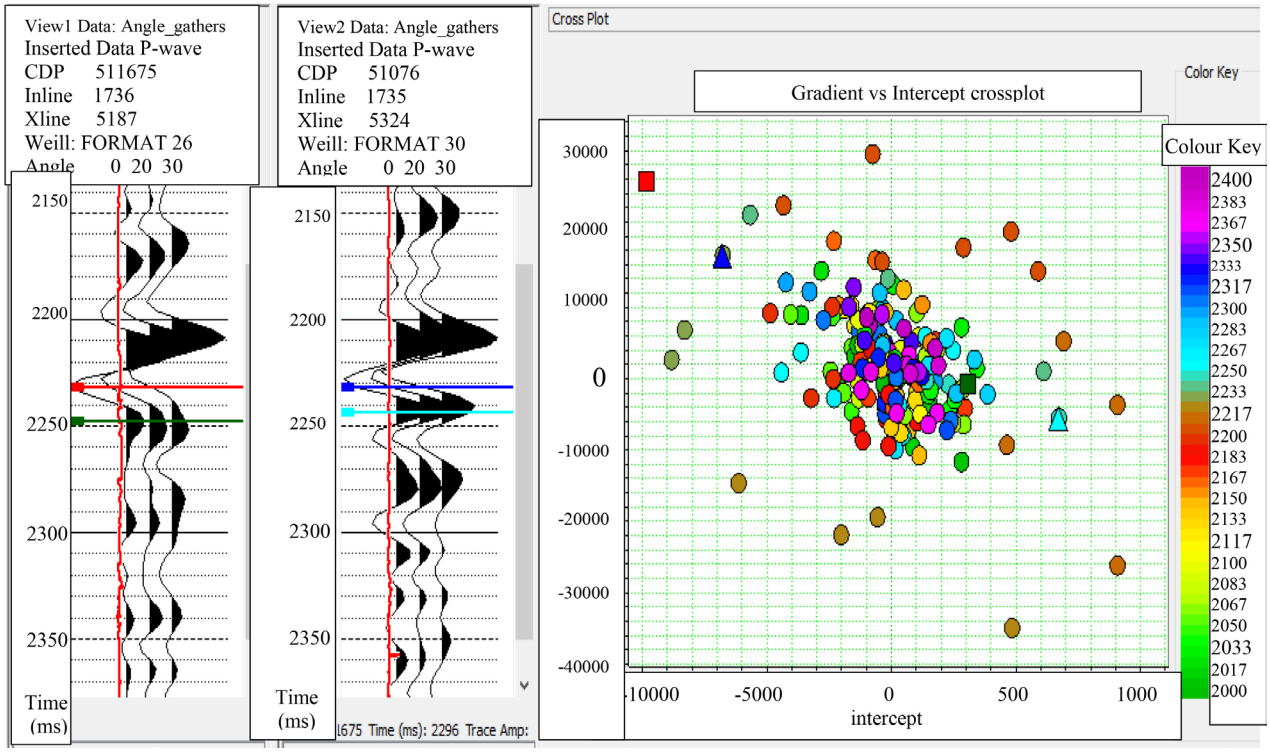

Figure 17. AVO scattered plot showing the Intercept vs Gradient (VOM 30 for top and bottom) of the pure oil top (blue) and pure gas top (red) cases.

well and 30 well. Table 4 shows A and B curves parameters for real gathers scenarios for FORMAT 26 and FORMAT 30.

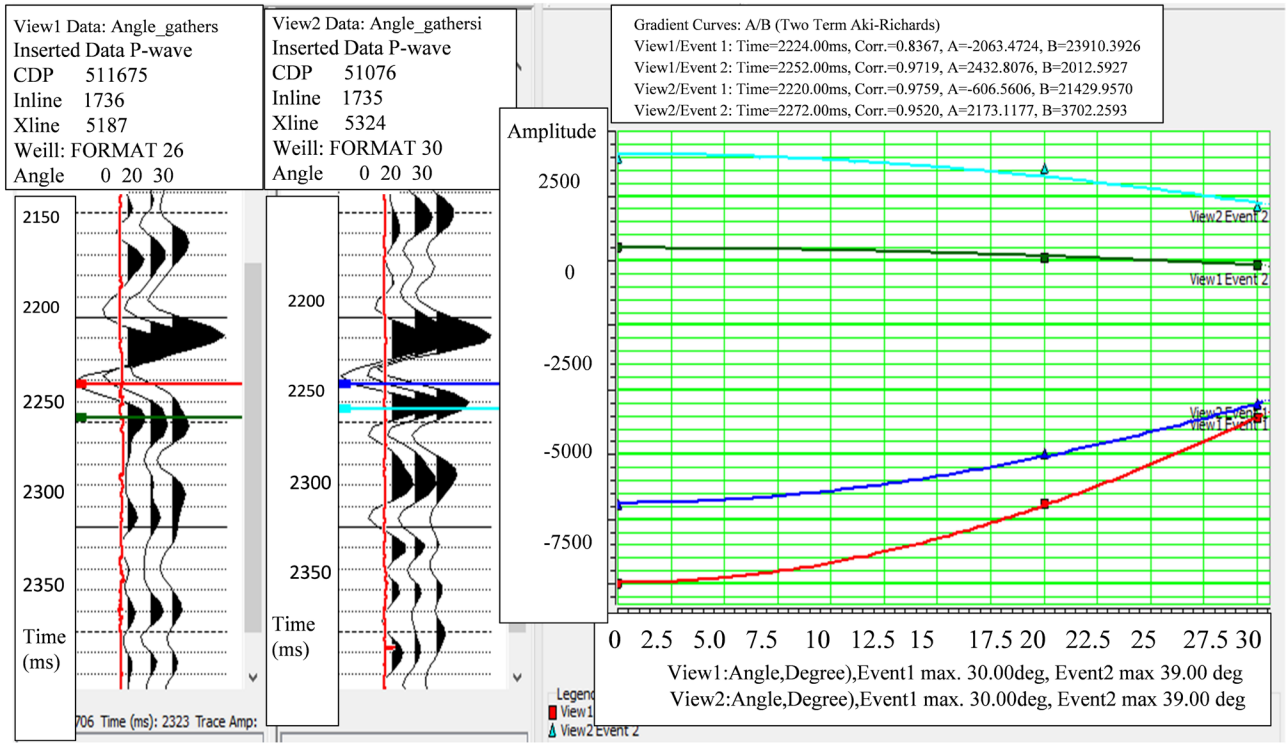

Figure 18. AVO cross plot showing the Intercept vs Gradient (VOM 30) for both top and bottom) of the pure oil top (blue) and pure gas top (red) cases.

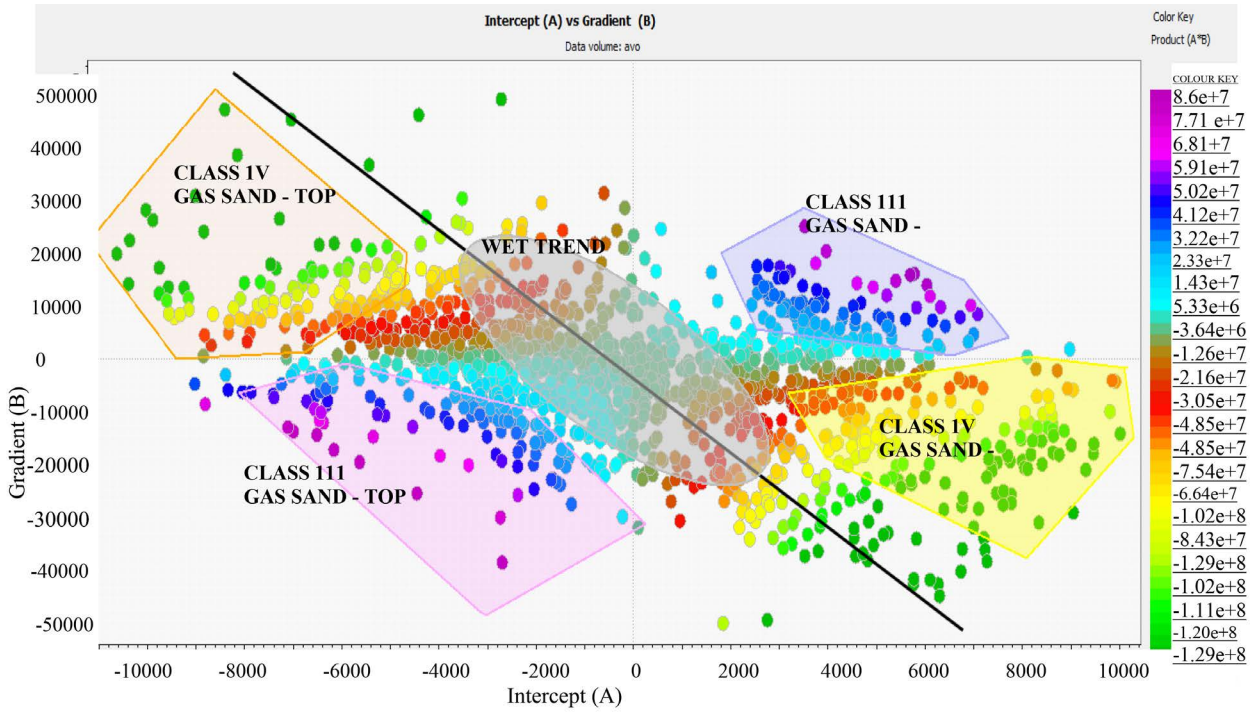

Figure 19. Crossplot for the intercept vs. gradient, illustrating the categories of different gas classes (III & IV).

3.3. AVO Attribute Volumes and Slices

The following results were obtained from the AVO attribute. The results are as

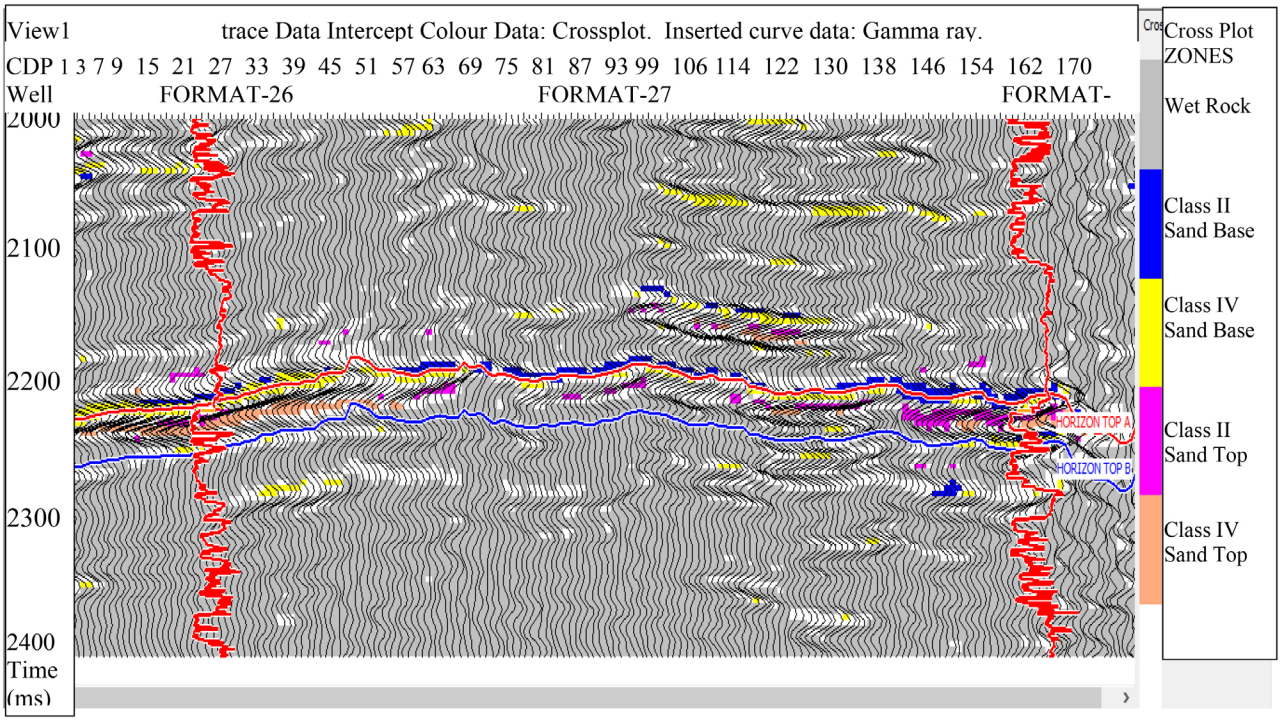

Figure 20. AVO crossplot superimpose on the volume showing two AVO anomalies of gas sand (class III and IV) of FORMAT sands at the FORMAT 26 well and 30 well.

Table 4. Intercept (A) and Gradient (B) parameters for real gathers scenarios for FORMAT 26 and 30.

Well	A (Intercept)	B (Gradient)	Correlation (%)	Time (ms)	Sand Interval
FORMAT 26	−2063.47	−23910.39	0.8367	2224	**Top**
	2432.80	2012.59	0.9719	2252	**Base**
FORMAT 30	−606.56	−21429.95	0.9759	2220	**Top**
	2173.11	3702.25	0.9520	2272	**Base**

shown in Figures 21-23. Figure 21 shows a scaled Poisson's ratio change (aA + bB), showing the decrease at stand top and positive base of AVO anomaly response of FORMAT sands at the FORMAT 26 and 30 wells. Figure 22 is a scaled S-wave Reflectivity (aA − bB), showing positive and negative at top and positive at base of AVO anomaly response of FORMAT sands at FORMAT 26 and 30 wells. Figure 23 is a product of the intercept and gradient (A × B), showing negative and positive at top and positive at base of AVO anomaly response of FORMAT sands at the FORAMT 26 and 30 wells.

4. Discussion

AVO Interpretation on Real Gathers

The top and base of the target zone at different well positions for FORMAT 26 and FORMAT 30 are plotted as AVO curves with intercept and gradient crossplot

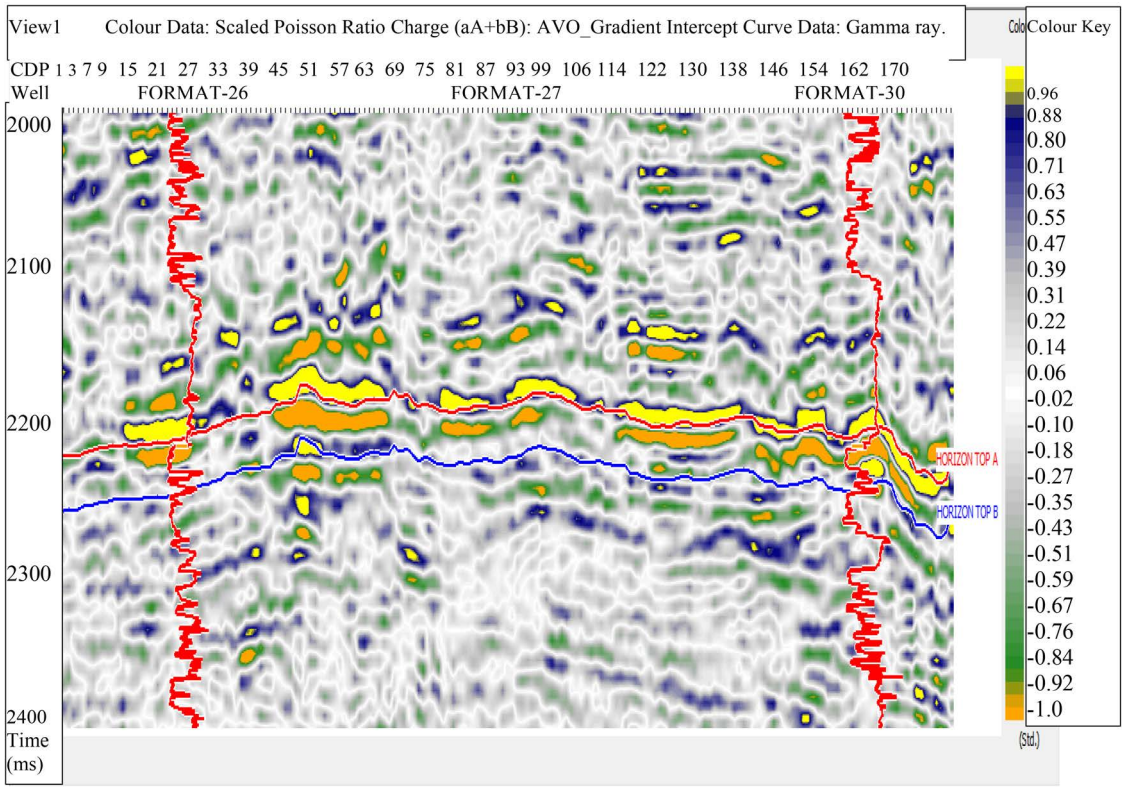

Figure 21. Scaled Poisson's Ratio change (aA + bB), showing the decrease at sand top and positive base of AVO anomaly response of FORMAT sands at the FORMAT 26 well and 30 well.

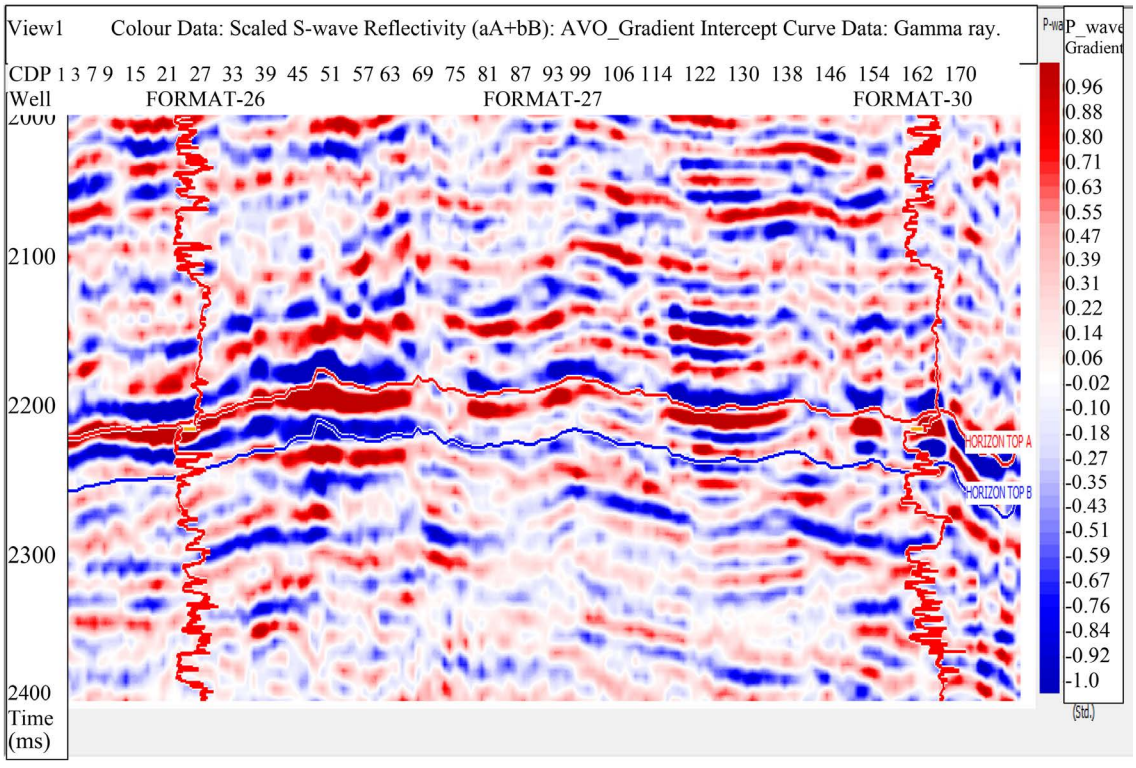

Figure 22. Scaled S-wave reflectivity (aA − bB), showing positive and negative at top and positive at base of AVO anomaly response of FORMAT sands at the FORMAT 26 well and 30 well.

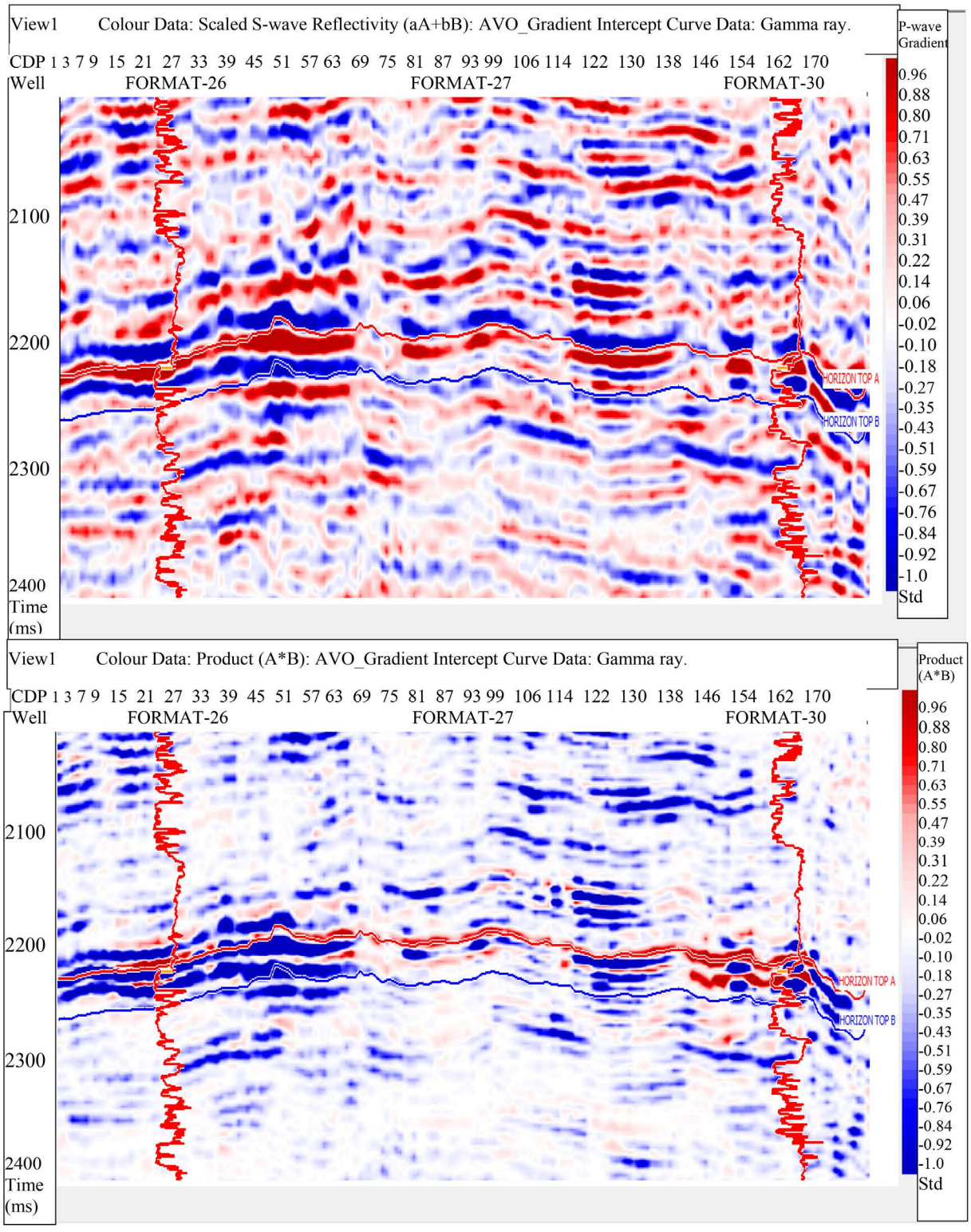

Figure 23. Product of the intercept and gradient (A × B), showing negative and positive at top and positive at base of AVO anomaly response of FORMAT sands at the FORMAT 26 well and 30 well.

space **Figure 18** using the two terms equation of [7], (Equation (1)) which the estimated parameters are summarized in **Table 4**. The AVO curves increasing

(brightening) with increase in offset (red/green curves-top) as the base curve dims with increase in offset (blue/cyan curves). The top of this AVO curve (red) plots at the class III position as the base (green) plots opposite it **Figure 17** having negative intercept (A = −2063) and gradient (B = −23910) for FORMAT 26. The top of this AVO curve (blue) increasing (brightening) with increase in offset as the base curve (cyan) dims with increase in offset. The top of AVO curve plots at the class II position as the base plots opposite it (**Figure 12**) has a negative intercept (A = −606) and gradient (B = −21,429) for FORMAT 30.

A practical approach adopted includes obtaining a crossplot of the intercept (A) and gradient (B) for all the time samples at all the trace locations within 2000 ms - 2400 ms time window. This has the significant advantage of providing the ability to consider more than, just the sample of the seismic event that has been picked. Information about an interface is contained in the whole wavelet, not just the peak or trough. Deviation from this regime may be a hydrocarbon indicator. The intercept and gradient pairs move more away from the background trend, with a decrease in the fluid density, so that gas sands will be the most well-separated **Figure 19**. AVO interpretation, using this technique, which was done in this study by: 1) defining the background trend around the origin (gray color); 2) the two points, which lie outside this trend, which have been highlighted (pink indicates top gas zone (Class III) and yellow indicates top-gas zone (Class IV), and 3) wet trend anomalies indicate brine zone (gray color). **Figure 19** shows the extracted AVO cross-plotting (intercept × gradient), where the three sections have a distinct clear different response between the gas bearing sand and the wet sand, while **Figure 20** shows overlay AVO crossplot volume on seismic data, where the zones anomalies illustrating the gas accumulations (Class III & IV) and brine sand (wet trend) are seen on the seismic data with their respective positions. Here the gas sand anomalies saturate the top of the reservoir indicated by gamma ray curves and the wet sand anomaly is seen as a background (gray color).

The AVO attributes represent the output, which can be obtained from the AVO analysis. The AVO response of the reflector can be described by two parameters: the intercept or reflectivity (amplitude) at the zero-offset and the gradient of the amplitude variation with offset. **Figure 21** & **Figure 22** illustrate the AVO response derived from the intercept and gradient volumes. In **Figure 21** is the scaled Poisson ratio attribute where very low Poisson ratio (−1.0 = orange color) denotes gas sand anomaly as the yellow color (0.96) denotes shale zone. In this figure, we have seen orange color at the top of the reservoir sand indicated by gamma ray curves. Above the gamma ray curve is the yellow color indicating shale zone.

In **Figure 22** that is, scaled S-wave reflectivity where red color (positive = 0.96) and blue color (negative = −1.0) indicate useful attribute for gas sand anomalies delineation. Such, class III gas sand with positive top and base as observed in **Figure 22** at the well locations.

The product of intercept and gradient attributes is presented in **Figure 23**.

The Product (A*B) is the "product stack". As negative values for A and B become positive when multiplied together, this method can give positive brightness to both the top and base of Class 3 anomalies. Class III gas sand will have negative intercept and gradient. Thus, when taking the product of the two will show positive. This is evident in **Figure 23** where the top is at positive value (red color).

5. Conclusions

The amplitude variation with offset analysis was applied in this study to evaluate the reservoir characteristics including the fluid properties to reduce drilling risk associated with relying only on traditional seismic data interpretation routine. The approach adopted involved delineating the reservoir sands, the hydrocarbon-saturated reservoir which lies approximately between TVD (ft) of 10,350 - 10,450. The AVO synthetic modelling was performed to account for fluid substitution with a range from 1.1 - 2.9 in which the density for pure gas decreased from 2.3 - 1.6 and that of pure oil from 2.3 - 1.8. Similarly, the density for the pure brine increased from 2.3 to 2.8. These are indications of a hydrocarbon reservoir. On the other hand, the Poisson pure gas with a range between 0.1 -0.4 decreased from 0.32 to 0.13. This was followed by the Poisson pure oil from 0.32 to 0.2 and lastly the Poisson pure brine from 0.32 to 0.26.

The real data analysis using both Intercept and gradient plots and AVO scattered plots revealed that the top and base conformed to the plot as in the case of the gas saturation. According to the Rutherford and William's (1989) classification model, the gas sand reservoir for FORMAT 26 is characterized by Class III AVO while FORMAT 30 is characterized by Class IV AVO.

The AVO Attribute volume slices using a color key between −0.1 to 0.96 show a decrease in the Poisson ratio from 0.96 to −1.0 which further indicated that the reservoir contained hydrocarbon. The S-wave reflectivity and the product of the Intercept and gradient further showed that there were Class 3 gas sand in the reservoir and another possible Class 4 gas sand anomaly in that same reservoir. Based on the result, the reservoir can be said to be of having high hydrocarbon potential. Consequently, the reservoir has been characterized to illuminate the reservoir constituents using the AVO analysis in the interpretation routine.

Acknowledgements

The authors acknowledge Shell Petroleum Development company Ltd. for supplying the data through the university assistance for the Department of Geology.

Conflicts of Interest

The authors declare that they have no competing interests.

References

[1] Eze, M.O., Mode, A.W. and Ugbor, C.C. (2013) Formation Evaluation of X7 Field in

the Niger Delta: Evidence from Petrophysical Data. Niger Delta, Nigeria. *IOSR Journal of Applied Geology and Geophysics* (*IOSR-JAGG*), **1**, 15-21. https://doi.org/10.9790/0990-0141521

[2] Ugbor, C.C. (2023) Evaluation of Hydrocarbon Reservoir in the "SIMA" Field of Niger Delta Nigeria from Interpretation of 3D Seismic and Petrophysical Log Data. *International Journal of Geosciences*, **14**, 94-107. https://doi.org/10.4236/ijg.2023.141006

[3] llo, C.A., Ugbor, C.C., Eradiri, J.N. and Emedo, C.O. (2022) Prospect Identification and Reservoir Characterization Using Seismic and Petrophysical Data in 'Famito' Field, Onshore Niger Delta, Nigeria. *Arabian Journal of Geoscience*s, **1**, Article No. 348. https://doi.org/10.1007/s12517-022-09615-0

[4] Ugbor, C.C. and Onyeabor, S.O. (2023) Assessment of the Spectral Decomposition Techniques in the Evaluation of Hydrocarbon Potential of "BOMS" Field, Coastal Swamp Niger Delta, Nigeria. *International Journal of Geosciences*, **14**, 655-676. https://doi.org/10.4236/ijg.2023.147035

[5] Ugbor, C.C., Ugwuoke, C.I. and Odong, P.O. (2023) Hydrocarbon Prospectivity and Risk Assessment of "Bob" Field Central Swamp Depobelt, Onshore Niger Delta Basin, Nigeria. *Open Journal of Geology*, **13**, 847-882. https://doi.org/10.4236/ojg.2023.138038

[6] Hussein, M., Abu El-Ata, A. and El-Behiry, M. (2019) AVO Analysis Aids in Differentiation between False and True Amplitude Responses: A Case Study of El Mansoura Field, Onshore Nile Delta, Egypt. *Journal of Petroleum Exploration and Production Technology*, **10**, 969-989. https://doi.org/10.1007/s13202-019-00806-2

[7] Aki, K. and Richards, P.G. (1980) Quantitative Seismology Volume 1: Theory and Methods. W. H. Freeman and Company, Maryland, 700.

[8] Young, K.T. and Tatham, R.H. (2007) Fluid Discrimination of Poststack "Bright Spots" in the Columbus Basin, Offshore Trinidad. *The Leading Edge*, **26**, 1508-1515. https://doi.org/10.1190/1.2821936

[9] Rutherford, S. and Williams, R. (1989) Amplitude-versus-Offset Variations in Gas sands. *Journal of Geophysics*, **54**, 680-688. https://doi.org/10.1190/1.1442696

[10] Dubey, A.K. (2012) Reservoir Characterization Using AVO and Seismic Inversion Techniques. *The 9th Biennial International Conference & Exposition on Petroleum Geophysics*, Hyderabad, 205-211.

[11] Ross, C.P. (2000) Effective AVO Crossplot Modeling: A Tutorial. *Geophysics*, **65**, 700-711. https://doi.org/10.1190/1.1444769

[12] Zhang, H. and Brown, R.J. (2001) A Review of AVO Analysis. *CREWES Research Report*, **13**, 357-380.

[13] Soroka, W.L., Fitch, T.J., Sickle, K.H.V. and North, P.D. (2002) Successful Production Application of 3-D Amplitude Variation with Offset: The Lessons Learned. *Geophysics*, **67**, 379-390. https://doi.org/10.1190/1.1468598

[14] Haase, A.B. (2004) Modelling of Linearized Zoeppritz Approximations. *CREWES Research Report*, **16**, 1-12.

[15] Young, K.T. and Tatham, R.H. (2007) Multiple AVO Analysis Techniques to Evaluate Pore Fluid Saturant of "Bright Spots" in Stacked Sections, Columbus Basin, Offshore Trinidad. *SEG Technical Program Expanded Abstracts*, 283-287. https://doi.org/10.1190/1.2792427

[16] Chung, B.H. and Lee, H.Y. (2008) AVO Analysis of 3-D Seismic Data Acquired in Heuksan Basin for Detecting Free Gas Zone. *Journal of the Korean Society of Min-*

eral and Energy Resources Engineers, **45**, 484-494.

[17] Zuheyr, K. and Canan, C. (2011) Amplitude versus Offset (AVO) Analysis Modeling in Hydrocarbon Exploration: A Case Study. *International Journal of Physical Sciences*, **6**, 908-916.

[18] Enikanselu, P.A. and Adekanele, A. (2012) Direct Detection of Hydrocarbon Reservoir Using AVO Technique Offshore Niger Delta. *Canadian Journal on Computing in Mathematics*, *Natural Sciences*, *Engineering and Medicine*, **3**, 261-269.

[19] Ugwu, S.A. and Nwankwo, C.N. (2014) Integrated Approach to Geopressure Detection in the X-Field, Onshore Niger Delta. *Journal of Petroleum Exploration and Production 499 Technology*, **4**, 215-231. https://doi.org/10.1007/s13202-013-0088-4

[20] Obiekezie, T.N. and Bassey, E.E. (2015) 3D Structural Analysis of Otu Field, Niger Delta, Nigeria. *Physical Science International Journal*, **7**, 114-126. https://doi.org/10.9734/PSIJ/2015/16512

[21] Asubiojo, T.M. and Okunuwadje, S.E. (2016) Petrophysical Evaluation of Reservoir sand Bodies in Kwe Field Onshore Eastern Niger Delta. *Journal of Applied Sciences and Environmental Management*, **20**, 383-393. https://doi.org/10.4314/jasem.v20i2.21

[22] Emina, R. and Obiadi, C.M. (2016) Evaluation and Prospect Identification in the Olive Field, Niger Delta Basin, Nigeria. *Journal of Petroleum & Environmental Biotechnology*, **7**, Article 1000284. https://doi.org/10.4172/2157-7463.1000284

[23] Farfour, M., Al-Shuhail, A., Gaci, S. and Abd El-Gelil, M. (2018) Amplitude Variation with Offset Application History in Middle East and North African Basins. *Journal of Seismic Exploration*, **27**, 301-318.

[24] Olawale, O.O., Ajayi, F.S. and Akeye, N.A. (2017) Evaluation of Petrophysical Properties for Reservoir Characterization of AK Field, Onshore Eastern Niger Delta, Southern Nigeria. *Journal of Mining and Geology,* **53**, 67-77.

[25] Loizou, N., Liu, E. and Chapman, M. (2008) AVO Analyses and Spectral Decomposition of Seismic Data from Four Wells West of Shetland, UK. *Petroleum Geoscience*, **14**, 355-368. https://doi.org/10.1144/1354-079308-724

[26] Kulke, H. (1995) Regional Petroleum Geology of the World. Part II. Gebruder Borntraeger, Berlin, 143-172.

[27] Roberts, D.G. and Bally, A.W. (2012) Regional Geology and Tectonics: Phanerozoic Passive Margins, Cratonic Basins and Global Tectonic Maps. Elsevier, 1196. https://doi.org/10.1016/B978-0-444-56357-6.00025-1

[28] Onojake, M.C., Osuji, L.C. and Abrakasa, S. (2015) Source, Depositional Environment and Maturity Levels of Some Crude Oils in Southwest Niger Delta, Nigeria. *Chinese Journal of Geochemistry*, **34**, 224-232. https://doi.org/10.1007/s11631-015-0035-9

[29] Oyedele, K.F., Ogagarue, D.O. and Mohammed, D.U. (2013) Integration of 3D Seismic and Well Log Data in the Optimal Reservoir Characterisation of Emi Field, Offshore Niger Delta Oil Province, Nigeria. *American Journal of Scientific and Industrial Research*, **4**, 11-21. https://doi.org/10.5251/ajsir.2013.4.1.11.21

[30] Selley, R.C. (2004) Petroleum Geology of Africa: New Themes and Developing Technologies. *Geological Magazine*, **141**, 749-750.

[31] Edigbue, P.I., Komolafe, A.A., Adesida, A.A. and Itamuko, O.J. (2014) Hydrocarbon reservoir Characterization of "Keke" Field, Niger Delta Using 3D Seismic and Petrophysical Data. *Standard Global Journal of Geology and Explorational Research*, **2**, 43-52.

[32] Tuttle, M.L., Charpentier, R.R. and Brownfield, M.E. (1999) The Niger Delta Petroleum System: Niger Delta Province, Nigeria, Cameroon, and Equatorial Guinea, Africa. USGS Open-File Report 99-50-H. https://doi.org/10.3133/ofr9950H

[33] Nwajide, C.S. (2013) Geology of Nigeria's Sedimentary Basins. CSS Bookshops Ltd., Lagos, 565.

[34] Aturamu Adeyinka, O., Ojo Adebayo, O., Adebayo Olajide, F. and Akinyemi Segun, A. (2015) Palynostratigraphic Analysis of the Agbada Formation (Nep-1 Well) Offshore, Eastern Niger-Delta Basin, Nigeria. *British Journal of Environmental Sciences*, **3**, 19-31.

[35] Ostrander, W.J. (1984) Plane Wave Reflection Coefficients for Gas Sands at Non-Normal Angles of Incidence. *Geophysics*, **49**, 1637-1648. https://doi.org/10.1190/1.1441571

[36] Castagna, J.P., Batzle, M.L. and Kan, T.K. (1993) Rock Physics-The Link between Rock Properties and AVO Response. In: Castagna, J.P. and Backus, M., Eds., *Offset-Dependent Reflectivity-Theory and Practice of AVO Analysis*, Society of Exploration Geophysicists, Houston, 135-171. https://doi.org/10.1190/1.9781560802624

[37] Castagna, J. P. and Swan, H.W. (1997) Principles of AVO Crossplotting. *The Leading Edge*, **16**, 337-344. https://doi.org/10.1190/1.1437626

[38] Singleton, S. (2011) The Effects of Seismic Data Conditioning on Prestack Simultaneous Impedance Inversion. https://doi.org/10.5724/gcs.11.31.0035

[39] Durrani, M.Z.A., Khan, M.R., Palekar, A. and Sarosh, B. (2017) A Pragmatic Approach for Prestack Seismic Data Conditioning and Quality Inspection for Quantitative Seismic Reservoir Characterization. *SEG Technical Program Expanded Abstracts*, 488-492. https://doi.org/10.1190/segam2017-17736663.1